UCRL-CR-116116
FINAL REPORT

SUPERPLASTICITY IN FINE-GRAINED CERAMICS

T.G. NIEH

This paper was prepared for:
U.S. ARMY RESEARCH OFFICE
Dr. Wilbur Simmons

January 31, 1994

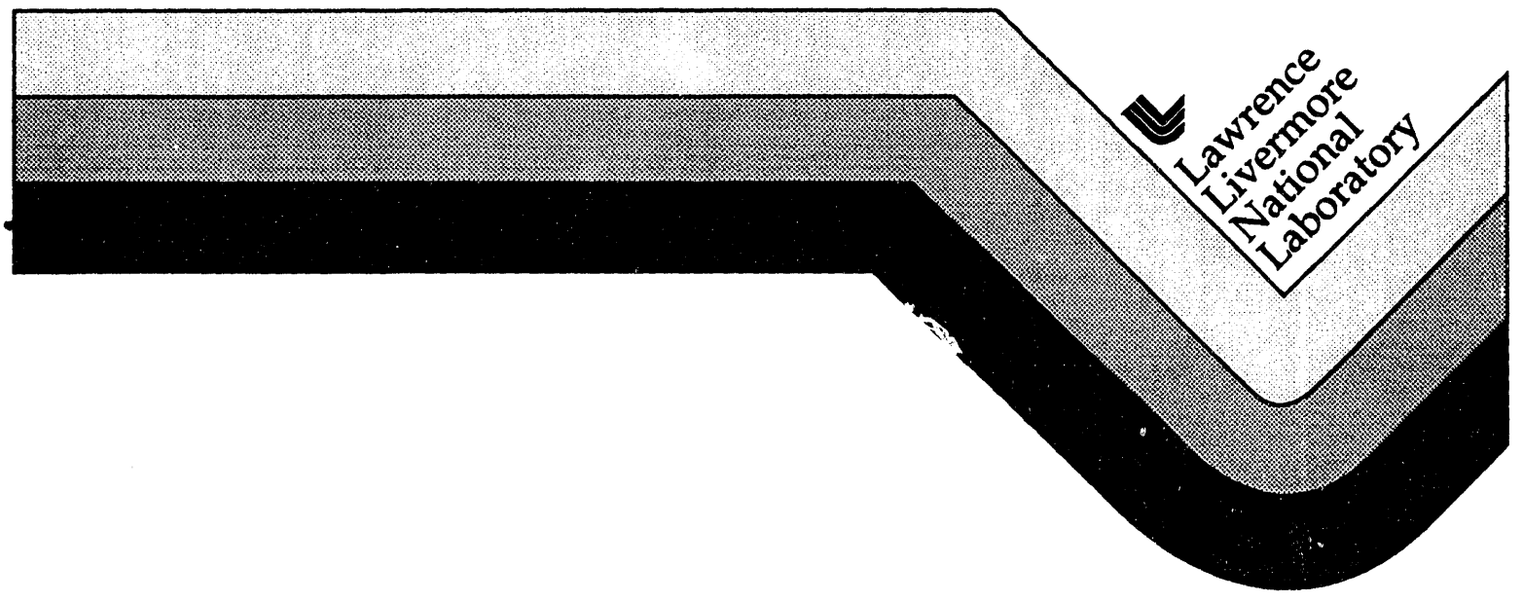

DISCLAIMER

REPORT DOCUMENTATION PAGE

Form Approved
OMB No. 0704-0188

1.AGENCY USE ONLY	2.REPORT DATE	3.REPORT TYPE AND DATES COVER
	January 31, 1994	Final Report 1 July 1993 to 31 December 1993

4.TITLE AND SUBTITLE

SUPERPLASTICITY IN FINE-GRAINED CERAMICS

5.FUNDING NUMBERS

MIPR

6.AUTHOR(S)

T.G. Nieh

7.PERFORMING ORGANIZATION NAME(S) AND ADDRESS(ES)

Lawrence Livermore National Laboratory
L-350, P.O. Box 808
Livermore, California 98350

8.PERFORMING ORGANIZATION REPORT NUMBER

UCRL-CR-116116

9.SPONSORING/MONITORING AGENCY NAME(S) AND ADDRESS(ES)

U.S. Army Research Office
P.O. Box 12211
Research Triangle Park, NC 27709-2211

10.SPONSORING /MONITORING AGENCY REPORT NUMBER

11.SUPPLEMENTARY NOTES

The view, opinions and/or finding contained in this report are those of the author(s) and should not be construed as an official Department of the Army position, policy, or decision, unless as designated by other documentation.

12a.DISTRIBUTION/AVAILABILITY STATEMENT

Approve for public release; distribution unlimited.

12b.DISTRIBUTION CODE

13.ABSTRACT (*Maximum 200 words*)

I. The superplastic deformation behavior of fine-grained, 20%alumina/yttria-stabilized tetragonal zirconia (20%Al_2O_3/YTZP) under conditions of biaxial gas-pressure deformation is described. Sheet specimens were deformed into hemispherical caps at temperatures ranging from 1450°C – 1600°C and at imposed gas pressures of 345 and 690 KPa. For the conditions examined, hemispherical caps were formed at times ranging from 1000 s to 2.1 x 10^4 s. The correlation between data obtained in uniaxial tensile testing and the behavior observed during the biaxial deformation experiments is discussed.

II. The high-temperature deformation behavior of a SiC whisker-reinforced, yttria-stabilized, tetragonal zirconia polycrystalline composite containing 20 vol.% SiC whiskers (SiC/Y-TZP) has also been investigated. Tensile tests were performed in vacuum at temperatures from 1450°C to 1650°C and at strain rates from 10^{-3} to 10^{-5} s^{-1}. The material exhibits useful high temperature engineering properties (e.g., ~100 MPa and 16% elongation at T = 1550°C and at a strain rate of ~10^{-4} s^{-1}). The stress exponent was determined to be $n \approx 2$. Scanning electron microscopy was used to characterize the grain size and morphology of the composites, both before and after deformation. Both dynamic and static grain growth were observed during deformation. The morphology of ceramic reinforcements appears to affect strongly the plastic deformation properties of Y-TZP. A comparison is made between the properties of monolithic Y-TZP, 20 wt.% Al_2O_3 particulate-reinforced Y-TZP (Al_2O_3/Y-TZP), and SiC/Y-TZP composites.

III Superplasticity deformation processing of ceramics has also been performed. Examples of biaxial gas-pressure forming of several ceramics, including yttria-stabilized, tetragonal zirconia (YTZP), a 20% alumina/YTZP composite, and silicon are given. In addition, the concurrent superplastic forming and diffusion bonding of a hybrid YTZP/C103 (ceramic-metal) structure are presented. These forming processes offer technological advantages of greater dimensional control and increased variety and complexity of shapes than is possible with conventional ceramic shaping technology.

14.SUBJECT TERMS

superplasticity, ceramics, ceramic composites, microstructures, grain boundary sliding, zirconia, alumina, rheology, forming, silicon carbide, high strain rate, metal matrix composites,

15.NUMBER OF PAGES

40

16.PRICE CODE

17.CLASSIFICATION OF REPORT	18.CLASSIFICATION OF THIS PAGE	19.CLASSIFICATION OF ABSTRACT	20.LIMITATION OF ABSTRACT
unclassified	unclassified	unclassified	Unlimited

SUPERPLASTICITY IN FINE-GRAINED CERAMICS

January 31, 1994

Lawrence Livermore National Laboratory
T.G. Nieh

Summary

During the performance of this report period, the technical progress has been summarized in three papers. The first two papers, entitled "Biaxial Gas-Pressure Forming of a Superplastic Al_2O_3/YTZP" and "Mechanical Properties of a 20 vol%SiC Whisker-Reinforced Yttria-Stabilized, Tetragonal Zirconia Composite at Elevated Temperatures", have been submitted in Journal of *Materials Engineering and Performance* and *Journal of Materials Research,* respectively, for publication. The third paper, entitled "Gas–Pressure Forming of Ceramic Sheet", was presented at the 3rd IUMRS-ICAM-93 Conference, in Tokyo, September 3, 1993, and will be included in the Conference Proceedings, to be published by Pergamon Press, Netherland.

CONTENTS

I. BIAXIAL GAS-PRESSURE FORMING OF A SUPERPLASTIC Al_2O_3/YTZP

(This paper, coauthored by T.G. Nieh and J. Wadsworth, has been submitted in *Materials Engineering and Performance* for publication, August, 1993.)

I-1 ABSTRACT

The superplastic deformation behavior of fine-grained, 20 wt% alumina/yttria-stabilized tetragonal zirconia (20 wt% Al_2O_3/YTZP) under conditions of biaxial gas-pressure deformation is described. Sheet specimens were deformed into hemispherical caps at temperatures ranging from 1450 to 1600°C and at imposed gas pressures of 345 and 690 KPa. For the conditions examined, hemispherical caps were formed at times ranging from 10^3 to 2.1×10^4 s. The correlation between data obtained in uniaxial tensile testing and the behavior observed during the biaxial deformation experiments of this study is discussed.

I-2 INTRODUCTION

Since it was initially reported in 1986 [1], the science of ceramic superplasticity has rapidly advanced. A variety of ceramic materials have been shown to exhibit superplastic behavior; these include yttria-stabilized tetragonal zirconia polycrystal [1-3], alumina [4], silicon nitride [4], hydroxyapetite [5], and composites of alumina-zirconia [6] and silicon nitride-silicon carbide [7]. For the most part, reports of ceramic superplasticity to date have focused on acquiring a fundamental understanding of ceramic superplasticity through uniaxial tension or compression testing. These studies have yielded invaluable information on the deformation behavior (e.g., strain rate sensitivity or stress exponent) and microstructural evolution (e.g., concurrent grain growth and cavitation behavior) of superplastic ceramics [8,9]. The knowledge of fundamental issues in ceramic superplasticity has now advanced to the stage that the technological application of superplastic deformation is beginning to receive increasing attention. Examples include successful extrusion of YTZP powders [10], closed die deformation of YTZP [11], punch forming of YTZP sheet [12] and, most recently, biaxial gas-pressure deformation of 20%Al_2O_3/YTZP [13], monolithic YTZP [14], and Fe/Fe_3C [15]. These forming processes offer technological advantages of greater dimensional control and increased variety and complexity of shapes than is possible with conventional ceramic shaping technology. This paper presents a

description of the superplastic forming behavior of 20%Al_2O_3/YTZP sheet under conditions of biaxial gas-pressure forming.

I-3 MATERIAL AND PROCEDURE

The material used in this study was a fine-grained YTZ containing 20 wt%Al_2O_3, (denoted Al_2O_3/YTZP, herein) obtained as 50 mm diameter discs, 1.5 mm in thickness, from Nikkato Corp., Japan. The microstructure exhibited an equiaxed YTZP grain size of 0.5 μm with a random distribution of 0.5 μm diameter Al_2O_3 grains. Data regarding the superplastic flow properties [16], grain growth behavior [17], and cavitation characteristics [18] of this 20%Al_2O_3/YTZP (under uniaxial tension conditions) have previously been reported. Based upon information from these previous studies, a gas-pressure forming apparatus was constructed with the capability to operate at temperatures of as high as 1700°C at gas-forming pressures of as high as 2.5 MPa. These forming pressures were chosen so as to impart true strain rates over the range of approximately 10^{-5} to 10^{-3} s^{-1}, within which Al_2O_3/YTZP exhibits the highest superplastic elongation. A detailed description of this apparatus has been presented elsewhere [14].

All experiments were conducted isothermally under conditions of constant applied forming pressure. Following equilibration at the temperature of interest, the desired forming pressure was applied and the resultant deformation monitored. Experiments were terminated when the deformation height corresponded to that of a hemisphere. The 50 mm diameter discs were clamped about their periphery resulting in an unconstrained diaphragm with a diameter of 38 mm. Thus, the height for deformation to a hemisphere was 19 mm.

Following deformation, all hemispheres were measured to determine the degree of deformation. These measurements were employed to determine true strain and average strain rate for each experimental condition. Strain distribution can be studied by two techniques: by sectioning formed articles or through the use of a grid system. The former technique is employed in the section which follows to describe the progressive deformation of a hemisphere. Use of the grid system involves placing an orthogonal grid system onto the undeformed diaphragm with the use of a diamond-tipped scribe and measuring the displacement of the grid subsequent to deformation. The grid technique provides reliable data on the in-plane strains with the through-thickness strains derived from these measurements through conservation of volume considerations.

I-4 RESULTS AND DISCUSSION

Six Al_2O_3/YTZP hemispheres superplastically deformed are shown in Fig.1-1. The hemispheres were deformed at forming pressures of 345 and 690 kPa, For the range of forming pressures and temperatures examined in this study, Al_2O_3/YTZP discs were deformed into hemispherical caps in times ranging from 10^3 to 2×10^4 s. As expected, a higher temperature and higher forming pressure result in a faster deformation.

The superplastic forming behavior for Al_2O_3/YTZP sheet at various temperatures and pressures is summarized in the deformation-time plots of Fig.1-2(a) and (b). The curves in Fig.1-2 indicate that there are essentially three distinct regions of behavior as deformation progresses for all the test conditions examined. Initially, the height of the deforming dome increases quite rapidly. This stage is followed by a period of "apparent" steady-state deformation, which is characterized by a minimum deforming rate. Finally, as the height approaches that of a hemisphere, the deformation rate increases again.

The three-stage behavior in Fig.1-2 appears to be similar to the creep curve of metal alloys deformed under a constant value of uniaxial stress, but its physical interpretation is quite different. This is because, although the applied pressure remained constant throughout the test, the resultant applied stress varies continuously during the course of deformation. In fact, the pressure-stress relationship for a deforming spherical thin shell follows the equation:

$$\sigma = \frac{P\rho}{2t} \qquad \text{eq.(1)}$$

where σ is the principal tangential stress acting in a shell having a wall of thickness t and radius ρ, and P is the applied gas pressure. For the experiments of this study, P remains constant, but ρ and t (and therefore σ) vary during the course of the test. Qualitatively, equation (1) predicts a high flow stress at the beginning of a test (when the radius, ρ, is very high) and at the end of a test (as the thickness, t, decreases). This results in a high forming rate at both low and high dome heights. As t and ρ are interdependent, the second stage of deformation occurs at a more-or-less constant rate because a decreasing radius is balanced by a decreasing shell thickness. Therefore, the three-stage behavior observed in Fig.1-2 not only results from the creep of the material, but also from the nature of biaxial forming.

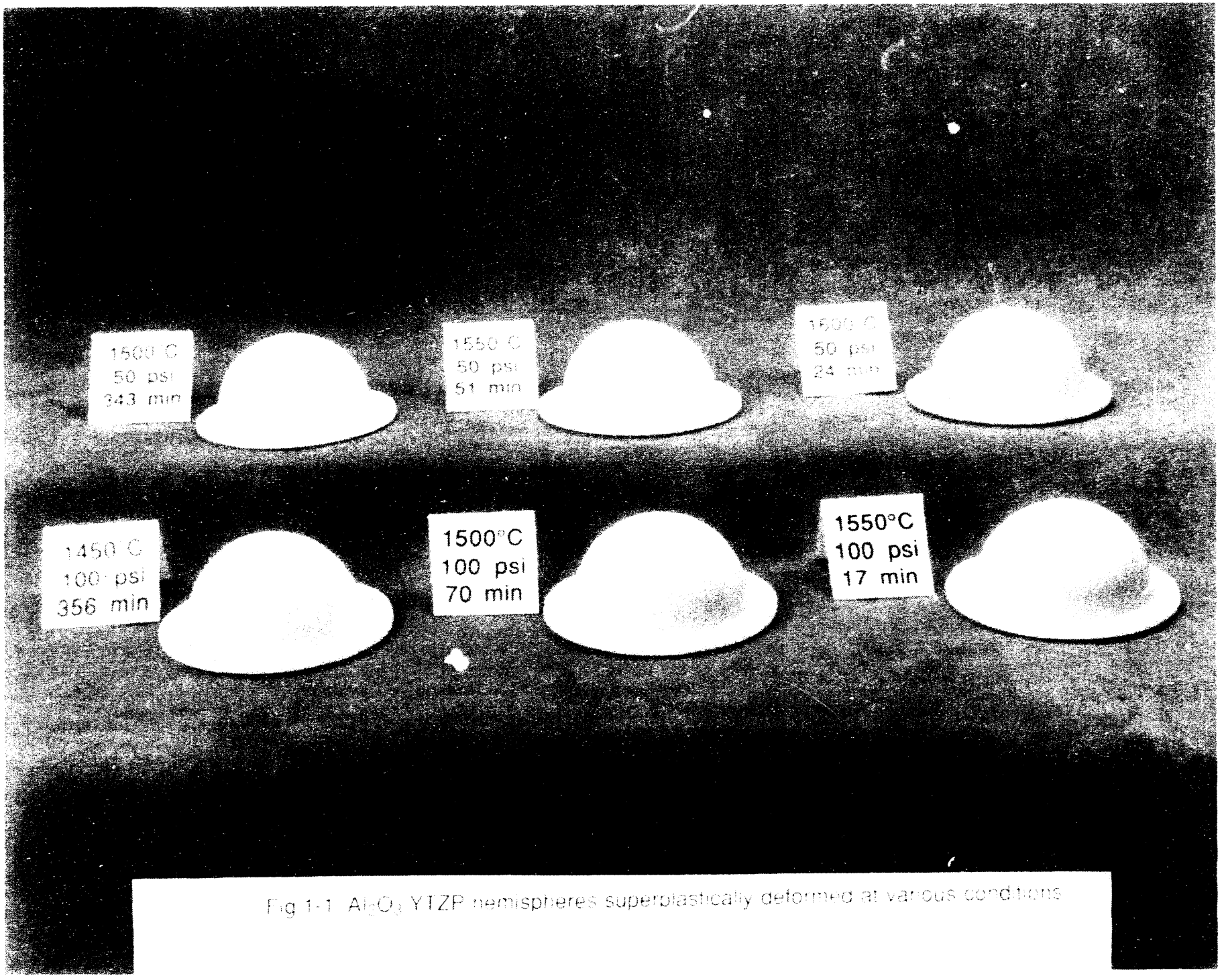

Fig 1-1 Al_2O_3 YTZP hemispheres superplastically deformed at various conditions

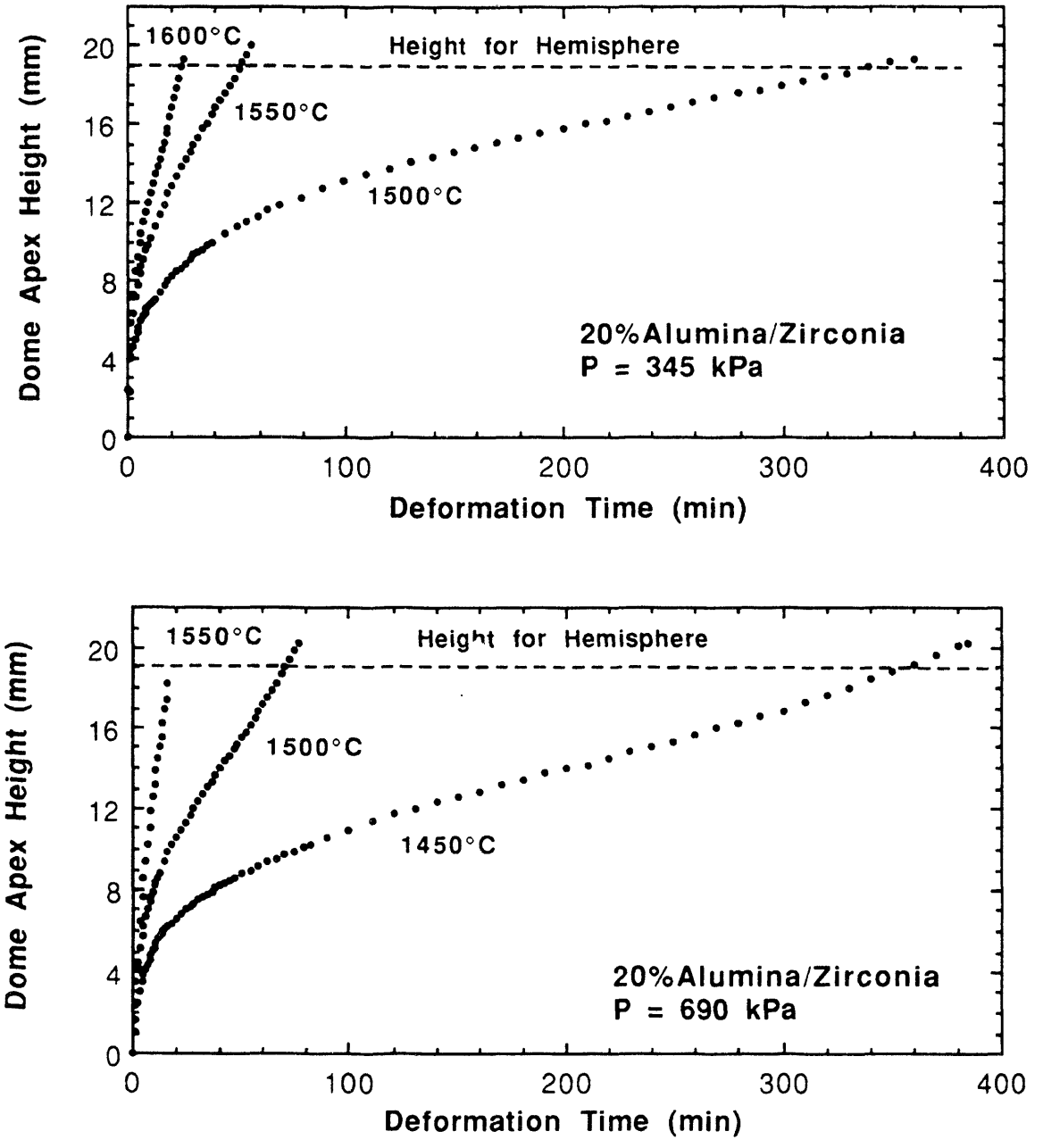

Fig.1-2 Superplastic forming behavior of Al_2O_3/YTZP sheet at (a) 345 KPa and (b) 690 KPa gas pressures.

To provide a more quantitative description of the relationship between σ, shell deformation, and strain rate, a mechanical analysis of the deformation process was performed. By assuming that the volume of the deforming shell remains constant, and that the thickness of the shell decreases uniformly during deformation, the flow stress acting in the shell may be determined through eq.(1). For the present experiments, the

radius ρ was deduced from the height of the deforming shell as measured and deduced from the contact LVDT sensor. The height of a deforming hemispherical cap may be related to its radius through a consideration of the cap geometry, as schematically shown in Fig.1-3.

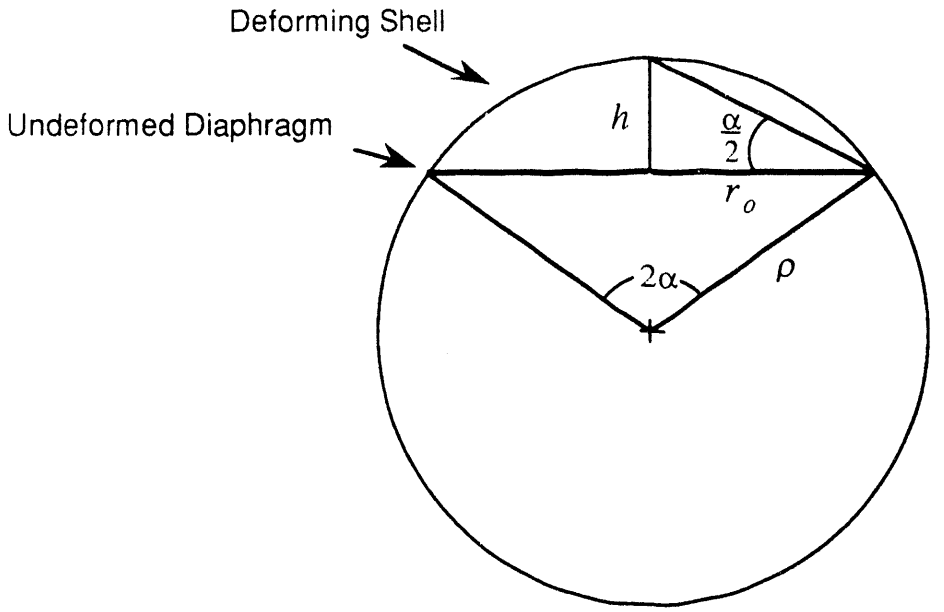

Fig.1-3 A hemispherical cap of height *h* and basal radius r_o may be considered to be a section of a sphere of radius *r* and included angle 2α.

A hemispherical cap of apex height, h, and base radius of, r_o, may be considered as a section of a sphere of radius ρ and included angle 2α. The included half-angle α may be determined by measuring the height h of the cap:

$$\tan\left(\frac{\alpha}{2}\right) = \frac{h}{r_o} \qquad \text{eq.(2)}$$

The radius ρ may then be determined as:

$$\rho = \frac{r_o}{\sin\alpha} \qquad \text{eq.(3)}$$

Knowledge of ρ and *h* together with the assumption that volume is conserved enables a determination of the average shell thickness $\bar{t}$:

$$\bar{t} = \frac{r_o^2 t_o}{2\rho h} \qquad \text{eq.(4)}$$

Equations (1–4) establish a relationship between the height of a deforming hemispherical shell and the flow stress acting in the shell wall.

For the present testing conditions, the relationship between σ and dome apex height has been calculated and is shown in Fig.1-4. For these calculations, the initial thickness, t, was 1.5 mm and the base radius r_0 was 19 mm. Note in Fig.1-4 that for each forming pressure, there exists a region in which a "nominal flow stress" acts for a large portion of the test. This region corresponds to the aforementioned "steady-state" deformation (region 2) observed in the deformation-time plots shown in Fig.1-2. The computed results presented in Fig.1-4 show that the nominal flow stresses for the experiments of this study were about 3.75 and 7.5 MPa for applied gas pressures of 345 and 690 KPa, respectively. Effective stresses are higher for a large radius (in the initial stages of forming) and diaphragm thinning (in the final stages of forming) regions. These calculations of variation in flow stress with increasing dome height agree with the general description of variation in deformation rate with increasing dome height, shown in Fig.1-2.

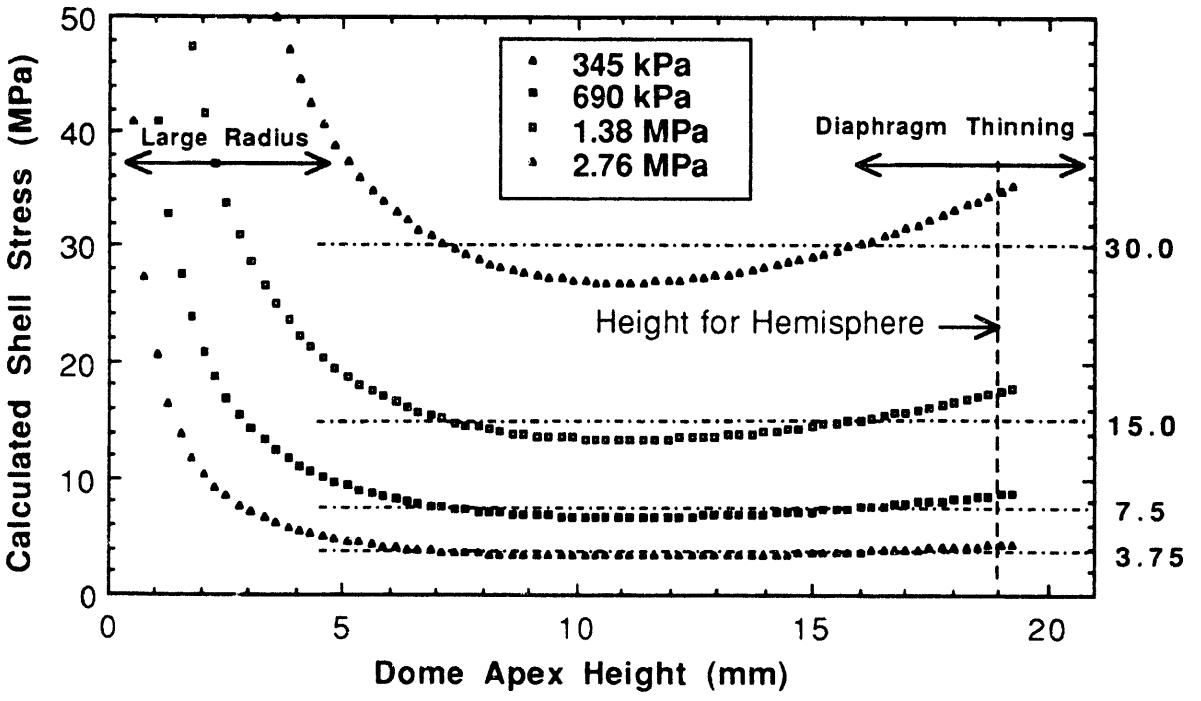

Fig.1-4 The relationship between σ and dome apex height.

In addition to the computed flow stresses for each experiment, the deformation strain rates were also estimated. As noted in Fig.1-2, the steady state also corresponds to the minimum strain rate region. The determination of this steady-state

strain rate as a function of the nominal stress, therefore, provides a first-order result of the biaxial forming properties. This is presented graphically as a log-log plot in Fig.1-5 Assuming a conventional power-law relationship, the minimum strain rate, $\dot{\varepsilon}$, can be expressed as:

$$\dot{\varepsilon} = B \cdot \sigma^n \qquad \text{eq.(5)}$$

where σ is the nominal stress, n is the stress exponent, and B is a constant. Despite limited data, the n value is approximately from 2 to 3, which is in the range for superplastic ceramics. Specifically, n is 3 at 1500°C, but decreases to about 2 at 1550°C.

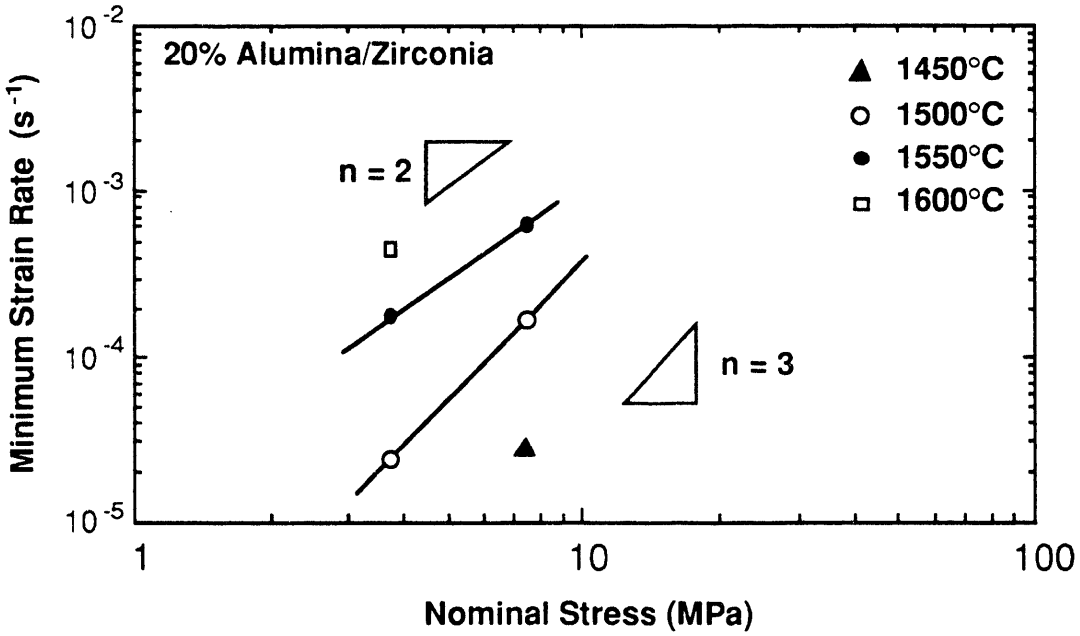

Fig.1-5 Minimum strain rate versus nominal stress for biaxial gas-pressure forming of Al_2O_3/YTZP.

It is of interest to compare the present results with those from uniaxial tests. Shown in Fig.1-6 is a direct comparison between the strain rate-stress data obtained from the present biaxial forming experiments at 1550°C and those from uniaxial tests [16]. It is particularly pointed out that the nominal stress, or stress for the biaxial tests used in Fig.1-5, is in fact the tangential stress. For the case of biaxial forming, and in the case of a spherical dome, the stress, as used in Fig.1-6, acting on the dome apex is the resultant stress of the tangential and circumferential stresses, which equals $\sqrt{2}$ of the stress value indicated in Fig.1-5. Taking into account this resultant stress would shift

the data in Fig.1-6 for the biaxial tests downward, thus moving them closer to the data for the uniaxial tests. However, the strain rate from the biaxial forming test is still about 3-4 times faster than that from the uniaxial tests. A faster strain rate was also observed during the biaxial gas-pressure forming of YTZP [14]. In fact, in the case of YTZP, the strain rate from the biaxial forming test is also about 3-4 times faster than that from the uniaxial tests.

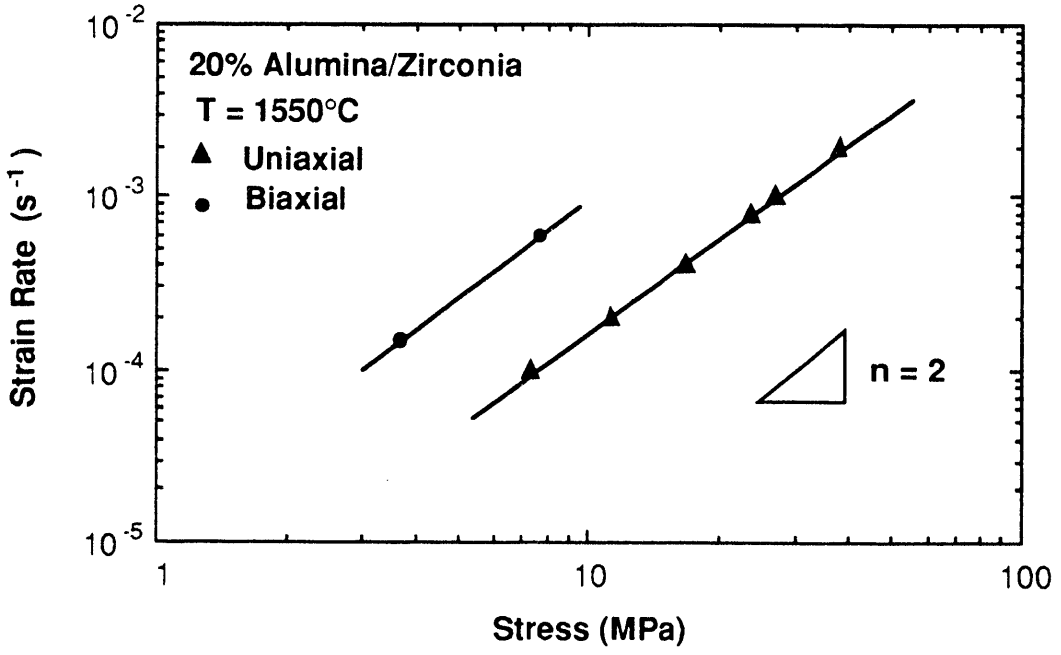

Fig.1-6 A direct comparison between the strain rate-stress data obtained from the present biaxial forming experiments at 1550°C and those from uniaxial tests.

Shown in Fig.1-7 is the cross section of a dome deformed at 1550°C. As expected, the thickness of the dome at each location varies. The thickness nonuniformity primarily arises from the variation in stress state from the clamped periphery of the diaphragm to its freely deforming center. At the center of the diaphragm is a stress state of equibiaxial tension (plane stress) described fully by eq. (1). At the clamped periphery of the diaphragm, however, is a state of plane strain. When the diaphragm is deformed by an applied gas pressure, the state of stress varies between the apex and the periphery. As a result of this stress gradient, deformation occurs under a corresponding strain rate gradient. The degree of thickness variation is determined by both the local stress and the strain rate sensitivity, m, where m = 1/n, of the deforming sheet. In the present case, thickness strain distributions of the deformed disk is shown in Fig.1-8, While the thickness of the periphery of the diaphragm is 1.5 mm, the thickness of the apex is only about 1.0 mm.

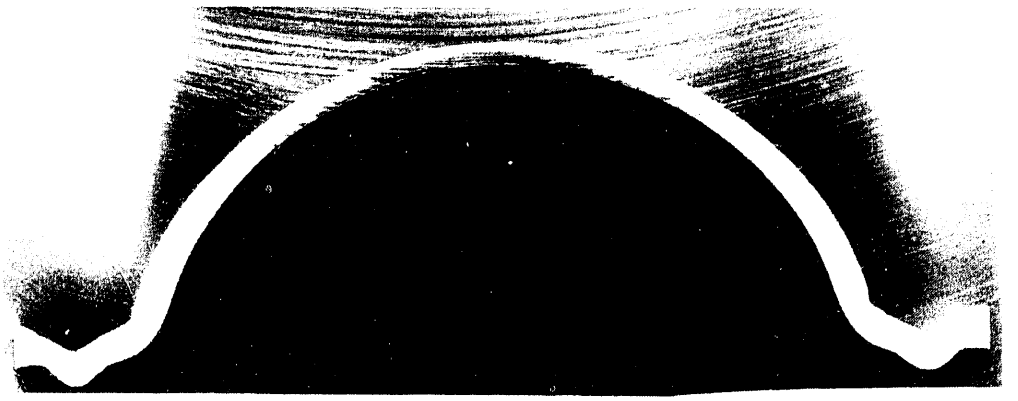

Fig.1-7 Cross section of a dome deformed at 1550°C.

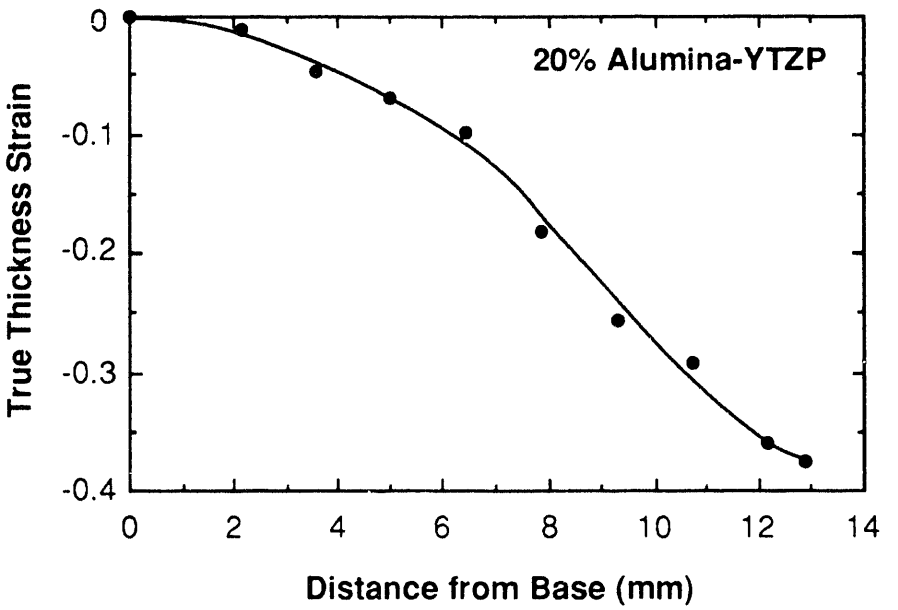

Fig.1-8 Strain distributions for the disk deformed at 1500°C and 690 kPa pressure.

Cornfield and Johnson (CJ) have developed a model to predict the thickness distribution for biaxial bulge forming [19]. The model was, however, derived under the condition of a constant m value, which is invalid for most superplastic ceramics. It has been reported that many superplastic ceramics, as a result of a fine grain size, undergoes severe dynamic grain growth during superplastic deformation, which changes the m value [8,9,20]. Therefore, a kinematic equation which incorporates

dynamic grain growth effects ultimately must be developed in order to predict precisely the strain distirbution.

I-5 CONCLUSION

A fine-grained 20wt%Al_2O_3/YTZP was successfully formed using a biaxial gas-pressure forming technique. Sheet specimens were deformed into hemispherical caps at temperatures ranging from 1450 to 1600°C and at imposed gas pressures of 345 and 690 KPa. For the forming conditions examined, hemispherical caps were formed at times ranging from 10^3 to 2.1×10^4 s. Mechanical analyses of the deformation process indicate that the stress exponent for deformation is approximately from 2 to 3. The strain rate from the biaxial forming test is about 3 to 4 times faster than that from the uniaxial tests,; this is similar to that observed during the biaxial forming of YTZP. The deformed domes exhibited a thickness variation from dome apex to dome base.

I-6 ACKNOWLEDGMENT

The financial support of this work was provided by the Army Research Office. The authors would like to thank Dr. J.P. Wittenauer for his technical contributions.

I-7 REFERENCE

1. F. Wakai, S. Sakaguchi, and Y. Matsuno, "Superplasticity of Yttria-Stabilized Tetragonal ZrO_2 Polycrystals," Adv. *Ceram. Mater.*, **1(3)**, (1986), pp. 259-263.

2. T.G. Nieh and J. Wadsworth, "Superplastic Behavior of a Fine-Grained, Yttria-Stabilized, Tetragonal Zirconia Polycrystal (YTZP),"*Acta Metall.*, **38**, (1990), pp. 1121-1133.

3. T. Hermansson, K.P.D. Lagerlof, and G.L. Dunlop, "Superplastic Deformation of YTZP Zirconia," in *Superplasticity and Superplastic Forming*, (ed. C.H. Hamilton and N.E. Paton), pp. 631-635; 1988, Warrendale, Pennsylvania, TMS.

4. I.W. Chen and L.A. Xue, "Superplastic Alumina Ceramics with Grain Growth Inhibitors," *J. Am. Ceram. Soc.*, **73(9)**, (1990), pp. 2585-2609.

5. F. Wakai, Y. Kodama, S. Sakaguchi, and T. Nonami, "Superplasticity of Hot Isostatically Pressed Hydroxyapatite," *J. Amer. Ceram. Soc.*, **73[2]** (1990), pp. 257-260.

6. T.G. Nieh, C.M. McNally, and J. Wadsworth, ","Superplastic Behavior of a 20% Al_2O_3/YTZ Ceramic Composite," Scr. *Metall.*, **23**, (1989), pp. 457-460.

7. F. Wakai, Y. Kodama, S. Sakaguchi, N. Murayama, K. Izaki, and K. Niihara, "A Superplastic Covalent Crystal Composite," *Nature*, **344**, (1990), pp. 421-423.

8. T.G. Nieh and J. Wadsworth, "Dynamic Grain Growth in Yttria-Stabilized Tetragonal Zirconia during Superplastic Deformation," J. *Amer. Ceram. Soc.*, **72[8]**, (1989), pp. 1469-1472.

9. D.J. Schissler, A.H. Chokshi, T.G. Nieh, and J. Wadsworth, "Microstructural Aspects of Superplastic Tensile Deformation and Cavitation Failure in a Fine-Grained, Yttria Stabilized, Tetragonal Zirconia," Acta *Metall. Mater.*, **39(12)**, (1991), pp. 3227-3236.

10. B. Kellett, P. Carry, and A. Mocellin, "Extrusion of Tet-ZrO_2 at Elevated Temperatures," in *Superplasticity and Superplastic Forming*, (ed. C.H. Hamilton and N.E. Paton), pp. 625-630; 1988, Warrendale, Pennsylvania, The Minerals, Metals, and Materials Society.

11. F. Wakai, ",A Review of Superplasticity in ZrO_2-Toughened Ceramics" *Brit. Ceram. Trans. J.*, **88**, (1989), pp. 205-208.

12. X. Wu and I.W. Chen, "Superplastic Bulging of Fine-Grained Zirconia," *J. Am. Ceram. Soc.*, **73**, (1990), pp. 746-749.

13. J.P. Wittenauer, T.G. Nieh, and J. Wadsworth, "A First Report on Superplastic Gas-Pressure Forming of Ceramic Sheet," *Scripta Metall. Maters.*, **26(4)**, (1992), pp. 551-556.

14. J. P. Wittenauer, T.G. Nieh, and J. Wadsworth, "Superplastic Gas-Pressure Deformation of YTZP Sheet," *J. Am. Ceram. Soc.*, **76**, (1993) pp. 1665-1672.

15. O.D. Sherby, Stanford University, private communication, (1993).

16. T.G. Nieh and J. Wadsworth, "Superplasticity in Fine-Grained 20%Al_2O_3/YTZ Composite," *Acta Metall. Mater.*, **39(12)**, (1991), pp. 3037-3045.

17. T.G. Nieh, C.M. Tomasello, and J. Wadsworth, "Dynamic Grain Growth in Superplastic Ceramics and Ceramic Composites," Symposium on *Superplasticity in Metals, Ceramics, and Intermetallics*, MRS Proceeding No. 196, pp. 343-348, edited by M.J. Mayo, M. Kobayashi, and J. Wadsworth, Materials Research Society, Pittsburgh, PA (1990).

18. A. Chokshi, D.J. Schissler, T.G. Nieh, and J. Wadsworth, "A Comparative Study of Superplastic Deformation and Cavitation Failure in a Yttria Stabilized Zirconia and a Zirconia Alumina Composite" Symposium on *Superplasticity in Metals, Ceramics, and Intermetallics*, MRS Proceeding No. 196, pp. 379-384, edited by M.J. Mayo, M. Kobayashi, and J. Wadsworth, Materials Research Society, Pittsburgh, PA (1990).

19. G.C. Cornfield and R.H. Johnson, "The Forming of Superplastic Sheet Metal," *Int. J. mech. Sci.*, **12**, (1970), pp. 479-490.

20. R. Raj, "Superplastic Deformation of Zinc Sulfide near Transformation Temperature (1020°C)," *J. Am. Ceram. Soc.* **72**, (199), pp. 1792-1796.

II. MECHANICAL PROPERTIES OF A 20 VOL%SIC WHISKER-REINFORCED YTTRIA-STABILIZED, TETRAGONAL ZIRCONIA COMPOSITE AT ELEVATED TEMPERATURES

(This paper, coauthored by S. E. Dougherty, T.G. Nieh, J. Wadsworth, and Y. Akimune, has been submitted in *Journal of Materials Research* for publication, August, 1993.)

II-1 ABSTRACT

The high-temperature deformation behavior of a SiC whisker-reinforced, yttria-stabilized, tetragonal zirconia polycrystalline composite containing 20 vol.% SiC whiskers (SiC/Y-TZP) has been investigated. Tensile tests were performed in vacuum at temperatures from 1450°C to 1650°C and at strain rates from 10^{-3} to 10^{-5} s^{-1}. The material exhibits useful high temperature engineering properties (e.g., ~100 MPa and 16% elongation at T = 1550°C and at a strain rate of ~10^{-4} s^{-1}). The stress exponent was determined to be $n \approx 2$. Scanning electron microscopy was used to characterize the grain size and morphology of the composites, both before and after deformation. The grain size in the composite was initially fine, but coarsened at the test temperatures; both dynamic and static grain growth were observed. The morphology of ceramic reinforcements appears to affect strongly the plastic deformation properties of Y-TZP. A comparison is made between the properties of monolithic Y-TZP, 20 wt.% Al_2O_3 particulate-reinforced Y-TZP (Al_2O_3/Y-TZP), and SiC/Y-TZP composites.

II-2 INTRODUCTION

One of the major drawbacks of using ceramics for engineering structures is low toughness at room temperature. As a result, many studies have been directed to the development of tough ceramics, with an emphasis on room temperature properties. Two major directions have been followed and it has now been established that ceramics can be toughened either by phase transformation induced by mechanical deformation [1] or by composite techniques [2-4]. The former mechanism is limited by the intrinsic phase stability of a given ceramic, whereas the latter mechanism, from an engineering viewpoint, appears to offer increased versatility. So far, several composite systems have been investigated [5]. In general, an improvement in the toughness of ceramics by a factor of two to three times can normally be obtained by

using a composite technique whereby a discontinous second phase is added to the primary matrix phase. Further toughness improvements will require, however, an increased understanding of the interfacial chemistry, structure, and bonding nature of the reinforcement and matrix phases. Despite strong interest in toughness improvement, the effect of second phase addition on mechanical properties, particularly at elevated temperatures, in ceramic composites has rarely been addressed [6-9].

In the present paper, high-temperature properties of a 20 vol% SiC whisker-reinforced yttria-stabilized tetragonal zirconia composite (denoted SiC/Y-TZP) will be presented and compared with those of monolithic yttria-stabilized tetragonal zirconia (Y-TZP) and another composite, 20 vol% Al_2O_3 particulate-reinforced Y-TZP (Al_2O_3/Y-TZP). The influence of the reinforcement morphology on the strength of composites will be discussed.

II-3 EXPERIMENTAL PROCEDURE

In the present study, an yttria-stabilized zirconia containing 20 vol% silicon carbide whiskers (SiC/Y-TZP) was produced by Nissan Motor Co. Ltd., Japan. The composite material was consolidated by vacuum hot pressing at 24.5 MPa and 1580°C for 1 h, from which in-plane, tensile coupons were machined. The processing procedures for the composite have been described previously [10]. The grain size of the Y-TZP matrix, measured from 50 scanning electron micrographs, was determined to be approximately 0.3-0.8 μm. SiC whiskers were expected to be randomly oriented in the plane perpendicular to the hot-press axis within the Y-TZP matrix. These whiskers were about 0.5 μm in diameter and were initially about 7.5 μm in length, but the length was reduced to approximately 6.5 μm (determined also from electron micrographs) as a result of consolidation.

To investigate the high-temperature deformation behavior of the SiC/Y-TZP composite, tensile specimens were tested in vacuum (10^{-3} Pa) at 1450°C, 1550°C, 1600°C, and 1650°C at nominal strain rates of 2×10^{-3}, 2×10^{-4}, and 8×10^{-5} s^{-1}. The test system was specially designed and constructed to include a vacuum type load cell which was actively cooled and located inside the vacuum system to bypass the vacuum bellows. This design permits a precise load measurement to ±0.45 N. The tensile fixture, which was essentially a universal joint with a pin-loading mechanism for the test sample, was made of thoriated tungsten and was designed to

minimize misalignment of the test system. The cross-head movement was monitored by a Hewlett-Packard computer equipped with a data aquisition system that controlled tests under either constant crosshead speed or constant true strain rate conditions. Machine compliance was calibrated at each of the test temperatures prior to testing. Tensile strain was subsequently determined from the crosshead displacement. These strain measurements were further confirmed by post-test measurements on the deformed samples. Due to sample availability, we only repeated one of the tests (8×10^{-5} s^{-1}, 1600°C) and the measured flow stresses were within ±10%. The microstructures, such as whisker morphology and average grain size, of the specimens prior to and after testing were characterized primarily using scanning electron microscopy (SEM).

II-4 RESULTS

II-4.1 Mechanical Properties

The true stress-true strain curve for a sample tested at 1550°C at a nominal strain rate of 2×10^{-4} s^{-1} is shown in Fig.2-1. It is noted that there exists very limited elasticity; the deformation of the material is almost completely plastic. The sample showed good high temperature flow strength, about 108 MPa, and a total elongation of approximately 16%. At increased temperatures and similar strain rates the material strength decreased and fracture strain increased only slightly. The general characteristics of the stress-strain curve shown in Fig.2-1 are typical of the stress-strain curves of all samples tested above 1450°C. The fracture strain of the composite is generally insignificant at 1450°C. It is particularly noted in Fig.2-1 that the curve shows extensive strain hardening and the absence of a steady state region. The initial strain hardening exponent is calculated to be about 0.85 which is similar to that for monolithic Y-TZP [11]. After the initial strain hardening region, the stress reaches a maximum around true strains of 0.10-0.14 after which the stress decreases before final fracture. The extent to which the stress decreases before final fracture was found to decrease at higher strain rates. At all testing temperatures the strength of the material decreased and the elongation to failure increased with decreasing strain rate. The largest recorded elongation to failure was 54% for a sample tested at 1600°C at a slow strain rate of 8×10^{-5} s^{-1}.

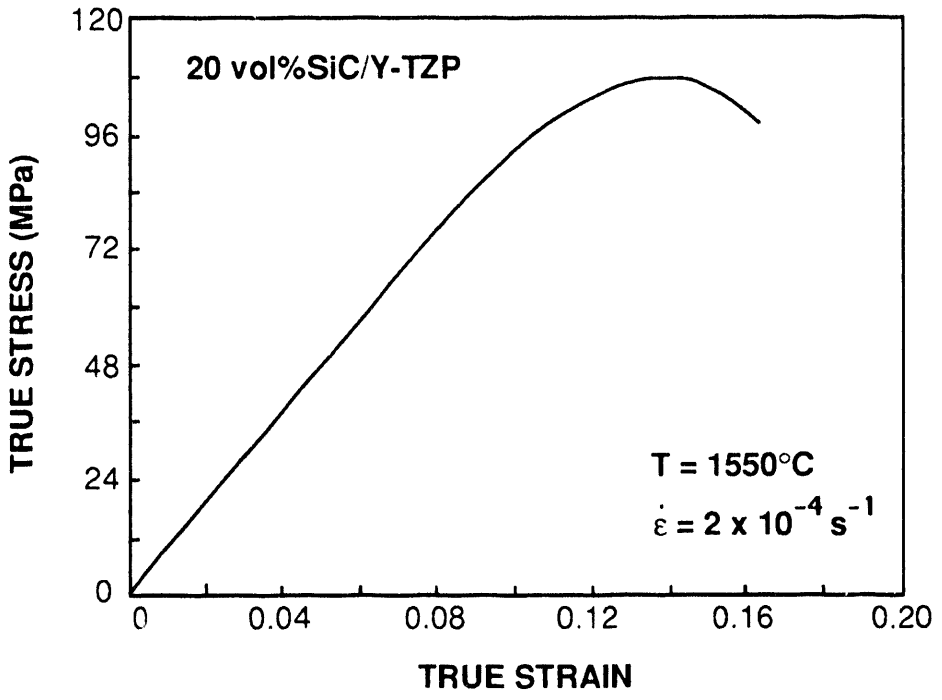

Fig.2-1 True stress-true strain curve for sample tested at 1550°C and a strain rate of $2 \times 10^{-4}\ s^{-1}$.

Dorn's equation has been traditionally used for describing the steady-state deformation of a material. In the present study, due to the absence of the steady state, it is difficult to rationalize the measured data. However, the physical basis for steady state is noted to be the constancy of microstructure resulting from the balance between work hardening and thermal softening. This microstructure, to a first order approximation, is expected to be a function of deformation strain, i.e, microstructure is nearly constant at a given strain. (Other microstructural parameters, such as grain shape, texture, interfacial bonding, subgrains, and dislocation density, are assumed to be independent of the test temperature and strain rate.) Therefore, despite the fact that our data did not reach steady state, the use of Dorn's equation is probably still the most sensible way to rationalize the measured data.

Consequently, to characterize the plastic flow behavior of the composite, the logarithm of initial (or nominal) strain rate is plotted as a function of the logarithm of peak flow stress for different temperatures in Fig.2-2. Despite some data scatter, the stress exponent value, n, in the equation

$$\dot{\varepsilon} = K \cdot \left(\frac{\sigma}{E}\right)^n \qquad (1)$$

where $\dot{\varepsilon}$ is the strain rate, σ is the stress, E is the Young's modulus, and K is a material constant, can be determined from Fig.2-2. (In Fig.2-2, σ, instead of (σ/E), is conveniently used because of the fact that the Young's modulus of Y-TZP is not a strong function of temperature [12].) The n values in Fig.2-2 are noted to vary with test temperature. Specifically, the n values are 3.0, 2.4, 1.6, and 1.8 for temperatures of 1450, 1550, 1600, and 1650°C, respectively. Except for the temperature of 1450°C, these n values are noted to be close to 2, indicating a mechanism of plastic flow that is often associated with grain boundary sliding [13].

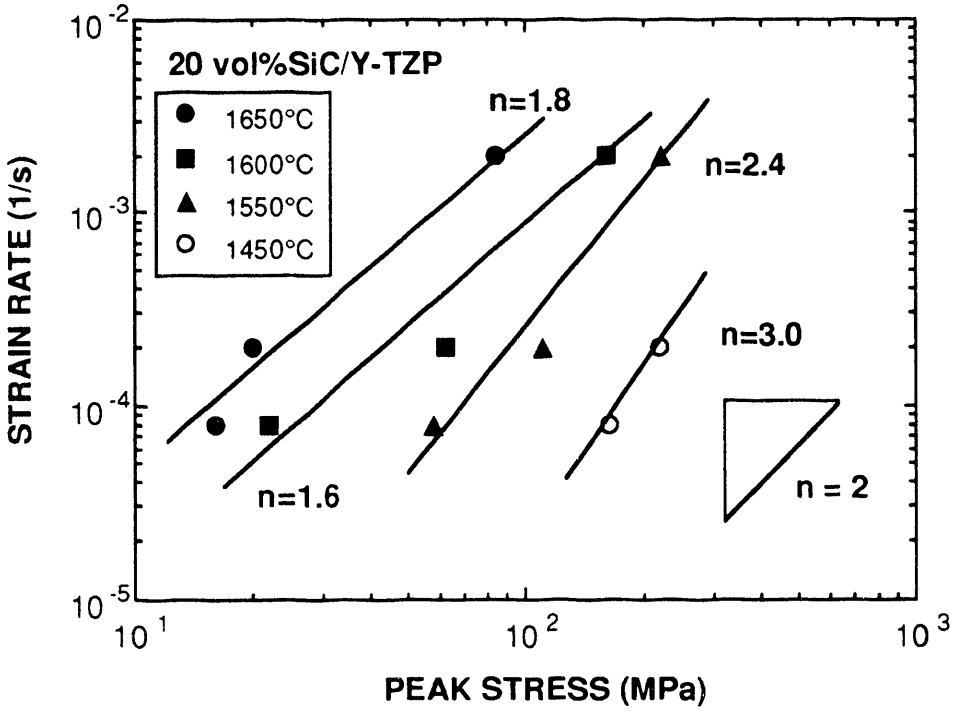

Fig.2-2 Strain rate as a function of peak flow stress for SiC/Y-TZP determined from constant true strain rate tests at different temperatures. The stress exponent, depending upon the test temperature, is about 2.0.

Assuming that the plastic flow in SiC/Y-TZP can be expressed as [13]:

$$\dot{\varepsilon} = A \cdot \left(\frac{\sigma}{E}\right)^n \cdot \exp\left(\frac{-Q}{RT}\right) \qquad (2)$$

where A is a material constant, Q is the apparent activation energy, R is the gas constant, and T is the absolute temperature. Using the data in Fig.2-2, the apparent activation energy can be calculated by plotting the logarithm of the stress-compensated strain rate, i.e., $\dot{\varepsilon}/\sigma^2$, versus reciprocal temperature as shown in Fig.2-3. (Again, σ, instead of σ/E, is used in Fig.2-3 for the activation energy measurement, because the Young's modulus of Y-TZP is not a strong function of temperature. In addition, the stress exponent is relatively low, thereby modulus has little effect on the accurate measurement of activation energy [14].) As shown in this figure, an average value of Q = 610 kJ/mol was obtained. It is interesting to point out that this Q value is close to the activation energy for superplasticity in Y-TZP, which was reported to be about 590 kJ/mol [15].

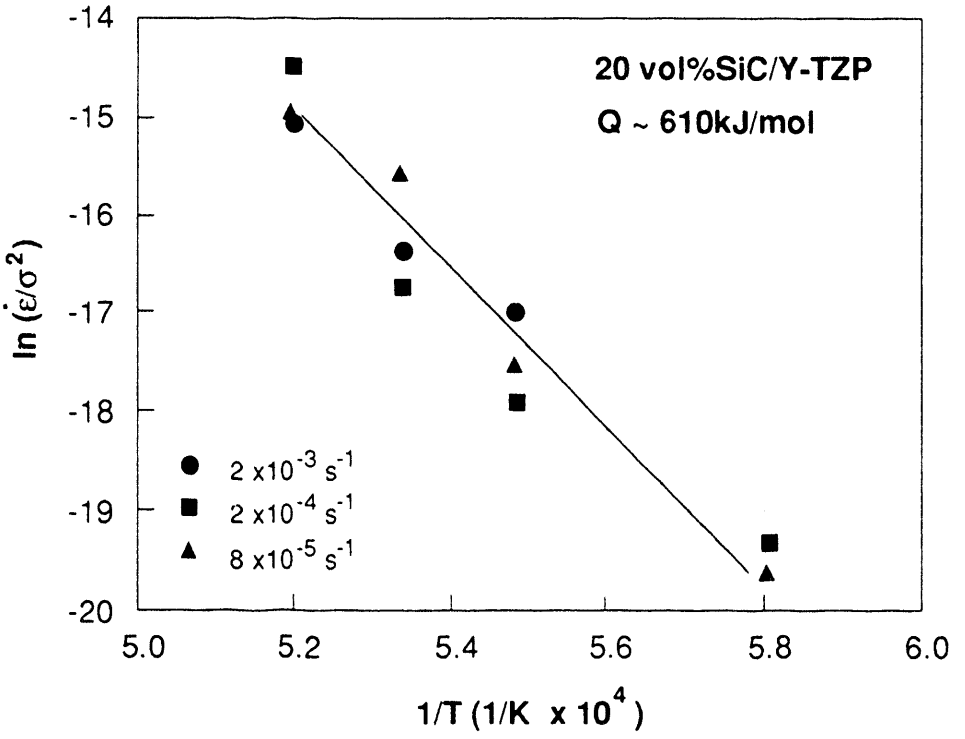

Fig.2-3 Arrhenius plot of the log of the stress-compensated strain rate as a function of inverse absolute temperature. The average apparent activation energy was determined to be about 610 kJ/mol.

II-4.2 Microstructure

Microstructural examination of the tested samples, using SEM, revealed that distinct, individual, SiC whiskers were randomly oriented within the Y-TZP matrix. X-ray diffraction from tested samples indicated the absence of a third phase, suggesting that if there exists any reaction between SiC and ZrO_2 it is insignificant. (Of course, this does not preclude the possibility of the presence of silica.) As shown in Fig.2-4, many whiskers are visible in the plane of the fracture. Large agglomerates of SiC were also observed in some areas on the fracture surface, as shown in Fig.2-5. This agglomeration is not expected to affect significantly the strength, but it can reduce the ductility of the material. All matrix grains remained virtually equiaxed after testing.

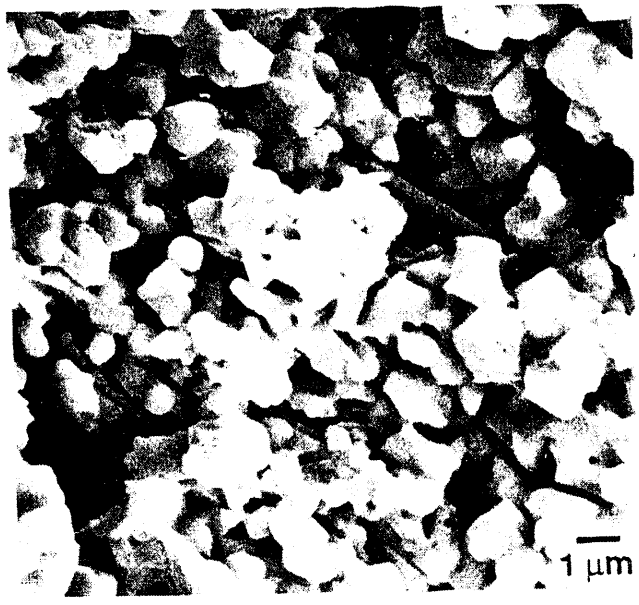

Fig.2-4 Microstructure of a tested SiC/Y-TZP sample showing that the SiC whiskers are randomly oriented within the Y-TZP matrix. Several fibers (marked by arrows) are visible in the plane of the fracture.

The microstructure of the composite appears to be thermally unstable. A comparison of the initial microstructure and those from the grip areas (representing static anneal) and the fracture surfaces (representing dynamic anneal) of the tested specimens showed that the microstructure coarsened at high temperatures. The grain size of the specimen increased with increasing testing temperature. For example, the average grain size in the grip (static) of the specimen tested at 1550°C and a strain

rate of 2×10^{-4} s^{-1} was approximately 1.0 μm, while the initial grain size of the sample was only about 0.3-0.8 μm. In addition to static grain growth, dynamic grain growth occurred; the average grain size in the gauge length (dynamic) of samples tested at 1550°C and 1650°C were 2.0 μm and 3.3 μm, respectively. The presence of SiC whiskers apparently has apparently little effect in inhibiting grain growth in Y-TZP. (In comparison, although initial grain size of the monolithic Y-TZP was 0.3 μm, it coarsened to 2.2 μm when the material was superplastically-deformed at 1550°C [11].) It is noted that dynamic grain growth has also been observed in monolithic Y-TZP [11] and Al_2O_3/Y-TZP [16].

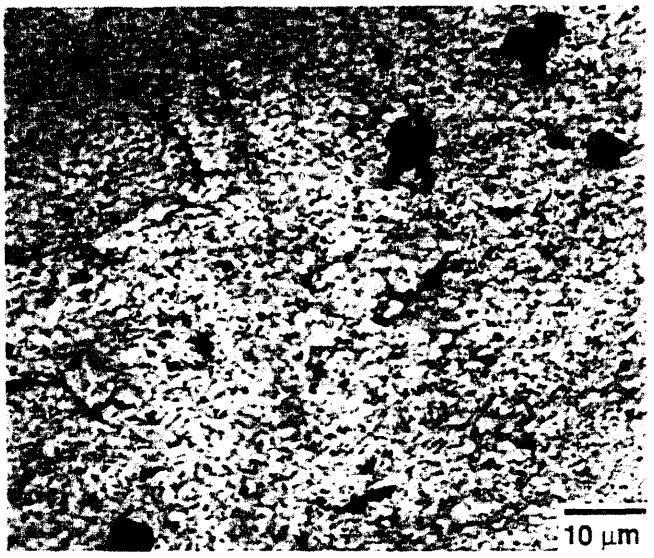

Fig.2-5 Large agglomerates (dark areas, marked by arrows) of SiC observed in some areas on the fracture surface. This agglomeration is not expected to affect significantly the strength, but it can reduce the ductility of the material.

All of the samples failed intergranularly. Extensive cavitation and/or surface microcracking was typically observed on the tested sample surfaces. The orientation of these microcracks appeared to be random; however, long microcracks running perpendicular to the tensile direction were often visible, in particular, in the gauge length near the final fracture location as shown in Fig.2-6. As a result of the extensive cavitation and microcrack formation, the tensile specimens exhibit virtually no macroscopic necking prior to fracture.

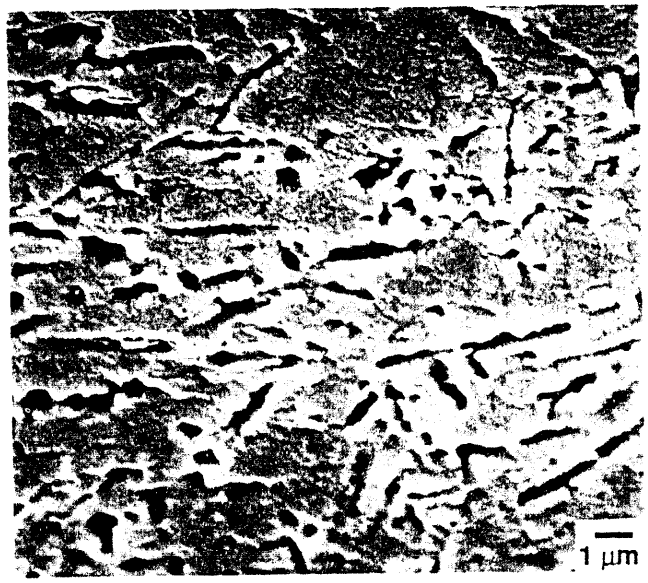

Fig.2-6 Extensive cavitation and/or surface microcracking observed on the tested sample surfaces. Long microcracks running perpendicular to the tensile direction are often visible in the gauge length near the final fracture location. Tensile axis is verticle in photomicrograph.

II-5 DISCUSSION

It is noted in Fig.2-1 that the stress-strain curve of the SiC/Y-TZP composite generally exhibits extensive work hardening and does not contain a steady state region; stress-strain curves for monolithic Y-TZP at elevated temperatures have similar characteristics [11,15]. Both the absence of a steady state region and extensive work hardening in the stress-strain curves of the SiC/Y-TZP are probably associated with concurrent grain growth during deformation in this material. It is known that the strength of a ceramic depends strongly upon the grain size, particularly for ceramics with a submicron grain size [17,18]. Grain growth also has a strong effect on the cavitation behavior in a material; a larger grain size can lead to more extensive cavitation, and thus less ductility.

An average stress exponent of $n \approx 2$ was measured for the SiC/Y-TZP composite. This corresponds to a strain rate sensitivity value of $m = 0.5$ ($n = 1/m$) which is

similar to the strain rate sensitivity values (m = 0.5-0.67) measured from monolithic Y-TZP [11,15]. This result suggests that plastic flow in the SiC/Y-TZP composite at elevated temperatures is primarily determined by the deformation of the fine-grained Y-TZP matrix. Namely, grain boundary sliding is the dominant deformation mechanism for both materials. This is further supported by the fact that the apparent activation energy for the SiC/Y-TZP composite (610 kJ/mol) is very close to the apparent activation energy for the monolithic Y-TZP, which is approximately 590 kJ/mol [15].

To illustrate the strength effect of SiC whiskers on Y-TZP, Fig.2-7 shows a comparison of SiC/Y-TZP and Y-TZP. It is apparent that the high temperature strength of Y-TZP was improved considerably by the addition of the SiC whisker reinforcements. For example, the peak flow stress measured from monolithic Y-TZP tested at 1550°C and a strain rate of 2.7×10^{-4} s^{-1} was about 16 MPa [11] compared to a peak flow stress of over 100 MPa measured from a SiC/Y-TZP specimen tested in the present study under similar conditions (1550°C, 2×10^{-4} s^{-1}). As discussed previously, the dominant deformation mechanism in Y-TZP and SiC/Y-TZP is essentially the same, i.e., grain boundary sliding. Plasticity in these two materials is, therefore, determined by the sliding mobility of grain (or particle) boundaries, not by the intrinsic (bulk) strengths of the grains. Therefore, although the intrinsic strength of SiC is greater than that of Y-TZP, the observed strengthening in SiC/Y-TZP composite is not caused by the strength of SiC *per se*. Rather, it results from the inhibition of grain (or particle) boundary sliding in the composite, caused by the presence of SiC whiskers.

To illustrate further the inhibition of grain boundary sliding caused by the presence of SiC whiskers, it is of interest to compare the plastic flow properties of the above two materials with another Y-TZP based composite, 20 wt% Al_2O_3 particulate-reinforced Y-TZP (Al_2O_3/Y-TZP) [16,19]. Data obtained from this composite are also included in Fig.2-7 for comparison. It is evident that, in contrast to SiC/Y-TZP, there is virtually no high-temperature strengthening as a result of the Al_2O_3 particulate addition to Y-TZP. It is important to point out that all the microstructural characteristics, except the morphology of reinforcements, are quite similar for the Al_2O_3/Y-TZP and SiC/Y-TZP composites; the matrix of both composites has equiaxed grains (or particles) with grain sizes of about 0.5 μm. The dominant deformation mechanisms for the monolithic Y-TZP, the Al_2O_3/Y-TZP and SiC/Y-TZP composites are also noted to be the same, i.e.,

grain boundary sliding. In fact, because of extensive grain boundary sliding, both the Y-TZP and the Al_2O_3/Y-TZP composite behave superplastically with maximum elongations of 800% and 625%, respectively. In contrast, the SiC/Y-TZP composite shows only moderate elongations (~50%) at similar elevated temperatures. Evidently, the morphology of reinforcements plays a vital role in determining the sliding mobility of the matrix, and thus the strength and ductility of a fine-grained composite.

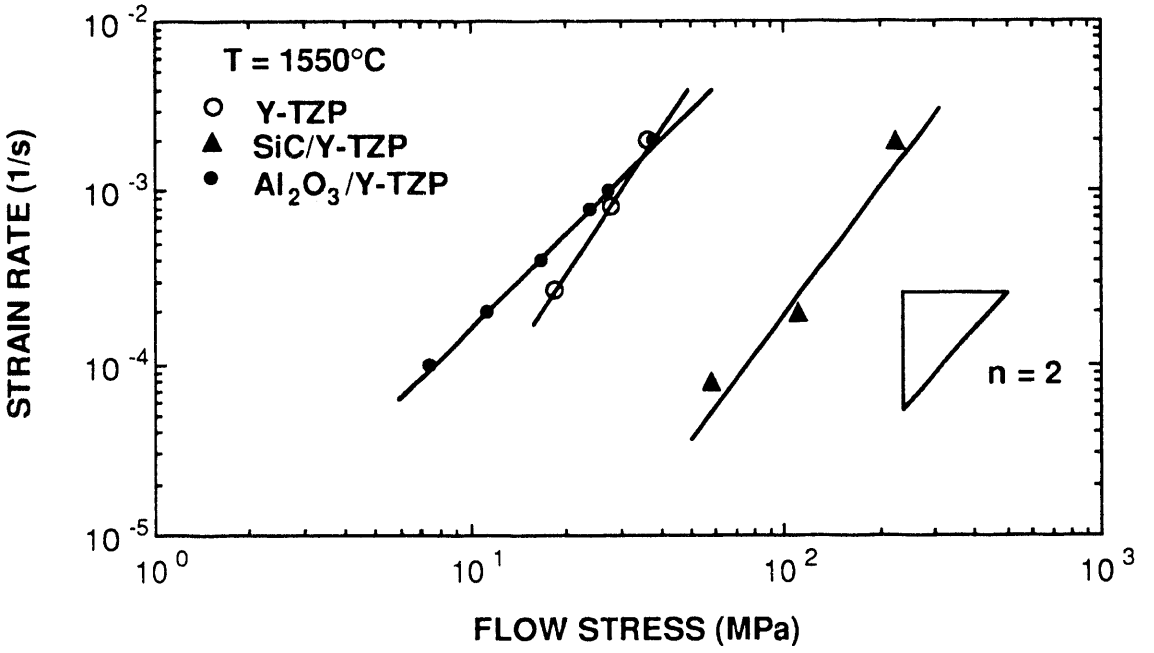

Fig.2-7 Direct comparison of the strengths of Y-TZP and SiC/Y-TZP and Al_2O_3/Y-TZP composites at 1550°C.

A rheological model to describe the strength of a ceramic containing rigid fiber reinforcements was proposed [9]. According to the model, for a matrix material that obeys a power law

$$\dot{\varepsilon} = \alpha(\sigma/ \sigma_o)^n \qquad (3)$$

where $\dot{\varepsilon}$ is the strain rate, σ is the stress, α is a reference strain rate, σ_o is a reference stress, and n is the stress exponent, a composite containing rigid fiber reinforcements follows a power law

$$\dot{E} = (1-V)^q \alpha(\Sigma/\sigma_o)^n \qquad (4)$$

where $\dot{E}$ is the strain rate of the composite, V is the volume fraction of the reinforcements, Σ is the macroscopic stress, and q is a constant, depending primarily upon the stress concentration factor.

In fact,

$$q = 1 + (k-1)n \qquad (5)$$

where k is the stress concentration factor. When the fiber reinforcements in a composite are parallel along the tensile stress axis,

$$k = 1 + (1/2+1/n)(L/R) \qquad (6)$$

where L and R are the half-length and the radius of the fiber reinforcement, respectively. When the reinforcements in a composite are spherical (or equiaxed),

$$k = 3/2 + 1/n \qquad (7)$$

In the present case of SiC/Y-TZP, since the SiC whiskers were randomly oriented in the plane perpendicular to the hot-press axis, the average concentration factor for uniaxial tension on this plane may be taken as one-half of Eq.(6) and one-half of Eq.(7), i.e.

$$k = 1 + (1/4 + 1/2n)(1 + L/R) \qquad (8)$$

This gives

$$q = 1 + (n/4 + 1/2)(1 + L/R) \qquad (9)$$

which, by substituting $L \approx 3.3\,\mu m$, $R \approx 0.25\,\mu m$, $V = 0.2$, and $n = 2$ into Eq.4, would lead to

$$(1-V)^q \approx 0.05$$

The strengthening factor, which is the inverse of $(1-V)^q$, is therefore approximately 20. This predicted value agrees reasonably well with the experimental result. As shown in Fig.2-7, the strain rate at a fixed flow stress for the SiC/Y-TZP composite is noted to be about 50 times smaller than that for the Y-TZP. The strengthening factor is quite sensitive to the volume fraction, the morphpology, and the orientation (with respect to the tensile axis) of the second phase. Small changes in the aspect ratio or volume fraction of the second phase greatly affect the strengthening factor. Strengthening by

equiaxed inclusions, for instance, becomes significant only at high volume fractions [9]. In the case of Al_2O_3/Y-TZP, the strengthening factor (derived directly using Eq.(7))

$$(1-V)^q \approx 0.4$$

which is relatively small and is difficult to verify experimentally. In fact, the data shown in Fig.2-7 indicate that the strengths of Y-TZP and Al_2O_3/Y-TZP are similar.

The tensile elongation of fine-grained ceramics at elevated temperatures generally decreases with increasing macroscopic flow stress [20,21]. This result is directly related to grain boundary cavity interlinkage in a direction perpendicular to the tensile axis of a ceramic during deformation [22]. When the flow stress is lower than the grain boundary strength of the material, intergranular failures do not occur and the material deforms plastically. As the flow stress is increased, so is the likelihood that the cohesive strength of grain boundaries will be reached. Once this level of stress is attained, intergranular cavitation and cracking occur, and the elongation to failure is decreased. In the case of the SiC/Y-TZP composites, the SiC whiskers have increased the material strength, and thereby the flow stress, by inhibiting the sliding of the Y-TZP grains. Thus, despite a relatively high strain rate sensitivity of m = 0.5, the SiC/Y-TZP composite exhibits only limited plasticity.

II-6 CONCLUSIONS

The addition of SiC whiskers to fine-grained Y-TZP results in a significant strengthening effect. As a result of the strengthening, the ductility of the composite is also reduced considerably. The strengthening does not result from the fact that SiC has a greater strength *per se*, but rather from the inhibition of grain boundary sliding caused by the presence of SiC whiskers. Apparently, the morphology of the reinforcements plays an important role in determining the strength of a composite. For example, at 1550°C and a strain rate of $10^{-3}\,s^{-1}$, the strengths of Y-TZP and 20 wt% (28 vol%) Al_2O_3 particle-reinforced Y-TZP are both less than 30 MPa, whereas the strength of 20 vol% SiC whisker-reinforced Y-TZP is almost 200 MPa. This is despite the fact that these three materials all have a fine-grained matrix (~0.5 μm). It is of interest to note that although the presence of SiC whiskers causes a dramatic strengthening effect, the dominant deformation mechanism in the SiC/Y-TZP composite is similar to that in the monolithic Y-TZP. Specifically, both materials deform by grain boundary sliding at elevated temperatures.

II-7 ACKNOWLEDGEMENTS

The financial support of this work was provided by the Army Research Office. The technical direction of Dr. Wilbur Simmons whose interest and enthusiasm for this project have been of great encouragement.

II-8 REFERENCES

1. P.F. Becher, "Toughening Behavior in Ceramics Associated with the Transformation of Tetragonal ZrO_2," *Acta Metall.*, **34**, 1885-1891 (1986).

2. J.-K. Guo, Z.-Q. Mao, C.-D. Bao, R.-H. Wang, and D.-S. Yan, "Carbon Fibre-Reinforced Silicon Nitride Composite," *J. Mater. Sci.*, **17**, 3611-16 (1982).

3. G.C. Wei and P.F. Becher, "Development of SiC-Whisker-Reinforced Ceramics," *Am. Ceram. Bull.*, **64[2]**, 298-304 (1985).

4. J.J. Brennan and K.M. Prewo, "Silicon Caride Fibre-Reinforced Glass-Ceramic Matrix Composites Exhibiting High Strength and Toughness," *J. Mater. Sci.*, **17**, 2371-83 (1982).

5. J.A. Cornie, Y-T. Chiang, D.R. Uhlmann, A. Mortensen, and J.M. Collins, "Processing of Metal and Ceramic Matrix Composites," *Amer. Ceram. Soc. Buil.*, **65**, 293-304 (1986).

6. A.H. Chokshi and J.R. Porter, "Creep Deformation of an Alumina Matrix Composite Reinforced with Silicon Carbide Whiskers," *J. Am. Ceram. Soc.*, **69 [2]**, C-144-C145 (1986).

7. H.T. Lin and P.F. Becher, "High-Temperature Creep Deformation of Alumina-SiC Whisker Composites," *J. Am. Ceram. Soc.* **74[8]**, 1886-93 (1991).

8. R. Duclos and J. Crampon, "Diffusion Creep of a SiC Whisker Reinforced Alumina/Zirconia Composite," *Scripta Metall.* **23**, 1673-78 (1989).

9. C.K. Yoon and I.W. Chen, "Superplastic Flow of Two-Phase Ceramics Containing Rigid Inclusions-Zirconia/Mullite Composites," *J. Am. Ceram. Soc.*, **73[6]**, 1555-65 (1990).

10. Y. Akimune, Y. Katano, and Y. Shichi, "Mechanical Properties and Microstructure of an Air-Annealed SiC-Whisker/Y-TZP Composite," *Adv. Ceram. Maters.* **3[2]**, 138-42 (1988).

11. T.G. Nieh and J. Wadsworth,"Superplastic Behavior of a Fine-Grained, Yttria-Stabilized, Tetragonal Zirconia Polycrystal (Y-TZP)," *Acta Metall. Mater.*, **38**, 1121-1133 (1990).

12. R. Stevens, Zirconia and Zirconia Ceramics, Magnesium Elektron Ltd., Twickenham, U.K.(1986).

13. J. Wadsworth and O.D. Sherby, "Superplasticity-Recent Advances and Future Directions"*Prog. Mater. Sci.*, **25**, 35-68 (1990).

14. A.H. Clauer and N. Hansen, "High Temperature Strength of Oxide Dispersion Strengthened Aluminum," *Acta Metall.*, **32**, 269-278 (1984).

15. F. Wakai, S. Sakaguchi, and Y. Matsuno, "Superplasticity of Yttria-stabilized Tetragonal ZrO_2 Polycrystals," *Adv. Ceram. Mater.*, **1[3]**, 259-63 (1986).

16. T.G. Nieh and J. Wadsworth, "Superplasticity in Fine-Grained 20%Al_2O_3/YTZ Composite," *Acta Metall. Mater.*, **39(12)**, 3037-3045 (1991).

17. T.G. Nieh and J. Wadsworth, "Effect of Grain Size on Superplastic Behavior of Y-TZP," *Scripta Metall. Mater.*, **24**, 763-766 (1990).

18. L.A. Xue and I.W. Chen, "Deformation and Grain Growth of Low-Temperature-Sintered High-Purity Alumina, " *J. Am. Ceram. Soc.*, **73[11]**, 3518-21 (1990).

19. F. Wakai and H. Kato, "Superplasticity of TZP/Al_2O_3 Composites," *Adv. Ceram. Mater.*, **3**, 71-76 (1988).

20. W.J. Kim, J. Wolfenstine and O.D. Sherby, "Tensile Ductility of Superplastic Ceramics and Metallic Alloys," *Acta Metall. Mater.*, **39**, 199-208 (1991).

21. I.-W. Chen and L.A. Xue, "Development of Superplastic Structural Ceramics," *J. Am. Ceram. Soc.*, **73**, 2585-2609 (1990).

22. D.J. Schissler, A.H. Chokshi, T.G. Nieh, and J. Wadsworth, "Microstructural Aspects of Superplastic Tensile Deformation and Cavitation Failure in a Fine-Grained, Yttria Stabilized, Tetragonal Zirconia," *Acta Metall. Mater.*, **39(12)**, 3227-3236 (1991).

III GAS–PRESSURE FORMING OF CERAMIC SHEET

(This paper, coauthored by T.G. Nieh and J. Wadsworth, has been presented at the 3rd IUMRS-ICAM-93 Conference, in Tokyo, September 3, 1993, and will be included in the Conference Proceedings, to be published by Pergamon Press, Netherland.)

III-1 ABSTRACT

Superplasticity in ceramics has now advanced to the stage that technologically viable superplastic deformation processing can be performed. In this paper, examples of biaxial gas-pressure forming of several ceramics are given. These include yttria-stabilized, tetragonal zirconia (YTZP), a 20% alumina/YTZP composite, and silicon. In addition, the concurrent superplastic forming and diffusion bonding of a hybrid YTZP/C103 (ceramic-metal) structure are presented. These forming processes offer technological advantages of greater dimensional control and increased variety and complexity of shapes than is possible with conventional ceramic shaping technology.

III-2 BACKGROUND

The forming of ceramics is generally difficult because the melting points of ceramics are relatively high and, consequently, the temperatures required to plastically deform ceramics are also high. The propensity for grain boundary separation in ceramics is also well-known. In the 1950s, extensive efforts were made in the western world and the former Soviet Union to hot fabricate ceramics using conventional metallurgical processes such as extrusion, rolling, and forging [1]. The goal was to produce near-net-shape parts in order to avoid expensive machining. A number of structural oxides, including CaO, MgO, SiO_2, ZrO_2, BeO, ThO_2, and Al_2O_3, were studied. As a result of this work, an improved understanding of ceramic deformation was developed but certain problems, and in particular the requirement for relatively high forming temperatures, still existed. For example, the temperature required for hot forging Al_2O_3 was found to be approximately 1900°C, which is extremely high from a practical standpoint. Subsequently, the concept of thermomechanical processing of ceramics was more-or-less abandoned.

Recent technical advances have changed this picture. First, advances in ceramic powder processing technology has greatly improved the quality of ceramic powders. High-purity ceramics of submicron grain size and more consistent microstructures are routinely prepared. Secondly, the observation that very fine-structure ceramic

materials can exhibit superplastic behavior has led to an intensive study of fundamental issues affecting the deformation behavior of ceramic materials. As a result, the science of ceramic superplasticity is now well-advanced with issues such as grain size effects [2], the role of grain boundary impurity [3], cavitation [4], concurrent grain growth [5], and elevated-temperature flow characteristics [6,7] well-documented for a number of ceramic systems. Improved understanding of these fundamental issues has advanced to the stage that technological application of ceramic superplastic deformation is receiving increasing attention. Examples include the extrusion of YTZP powders [8], closed die deformation of YTZP [9], punch forming of YTZP sheet [10] and, most recently, biaxial gas-pressure deformation of 20%Al_2O_3/YTZP [11], YTZP [12], and Fe/Fe_3C [13]. This paper presents examples of the superplastic forming of several ceramics via biaxial gas-pressure forming techniques, including YTZP, 20%Al_2O_3/YTZP, and silicon. In addition, we will present an example of the concurrent superplastic forming and diffusion bonding (SPF/DB) of a hybrid ceramic-metal (YTZP/C103) structure.

III-3 EXPERIMENTS

The equipment used to perform gas-pressure deformation has been described elsewhere [12]. The key features are shown in Fig.3.1. For all experiments, high-purity argon gas was used to impose the deformation pressure. In-situ deformation is measured when the diaphragm expands upwards to form a hemisphere; this displaces a silicon carbide sensor rod linked to an LVDT. The forming pressure was monitored both with a dial indicator as well as with an electronic DC strain gauge pressure transducer. The apparatus was inductively heated and fully enclosed within a vacuum chamber. A typical heat-up time was 30 minutes with a ten minute hold time prior to the application of forming pressure. All experiments were conducted isothermally under conditions of constant applied forming pressure and an ambient of 25 kPa argon. Materials for this study were in the form of 50 mm diameter discs, 1.5 mm in thickness. The discs were clamped at their periphery resulting in an unconstrained diaphragm with a diameter of 38 mm, producing a hemisphere of 19 mm in height.

III-4 RESULTS

III-4.1 Yttria-Stabilized, Tetragonal Zirconia Polycrystal (YTZP)

Forming experiments were conducted over a temperature range of 1450° to 1600°C and forming pressures in the range of 345 to 2760 kPa. These forming temperatures

and pressures were chosen to impart true strain rates over the range of approximately 10^{-5} to 10^{-2} s^{-1}.

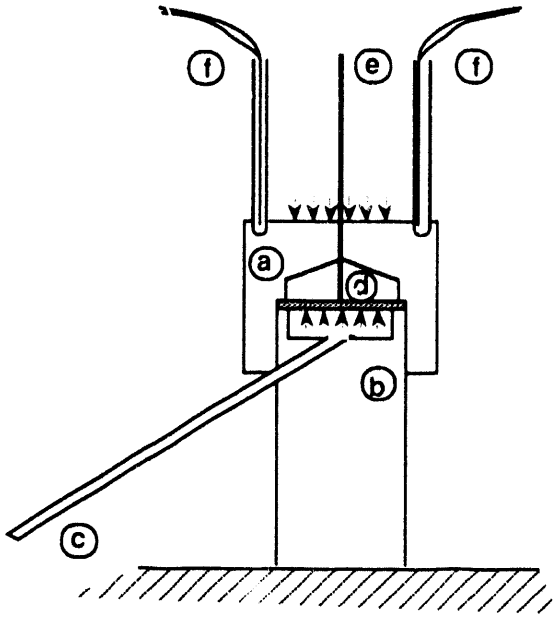

Fig.3-1 Gas-pressure forming apparatus. Upper die (a) and lower die (b). Gas is admitted through integral pressure tube (c), ceramic diaphragm (d) deforms upwards causing movement of deflection sensor (e). Temperature is monitored by twin thermocouples (f).

The forming behavior for YTZP sheet at a pressure of 690 kPa at various temperatures is summarized in the deformation-time plots of Fig.3.2. Data in Fig.3.2 exhibit three distinct regions of behavior as deformation progresses for each of the experimental conditions examined. Initially, the height of the deforming dome increases quite rapidly. This stage is followed by a period of apparent steady-state deformation. Finally, as the height approaches that of a hemisphere, the deformation rate increases again. The three-stage behavior shown in Fig.3.2 appears to be similar to the creep curve of metal alloys deformed under a constant value of uniaxial stress. In the present case, however, the interpretation is quite different. Although the applied forming pressure remains constant throughout the test, the resultant stress acting in the deforming shell varies continuously during the course of deformation. As the thickness and radius of a deforming shell are interdependent, the second stage of deformation occurs at an approximately constant rate because the decreasing radius of curvature is balanced by the decreasing shell thickness. In fact, the three–stage

behavior observed in Fig.3.2 not only results from the creep of the material but also from the nature of constant–pressure biaxial forming [12].

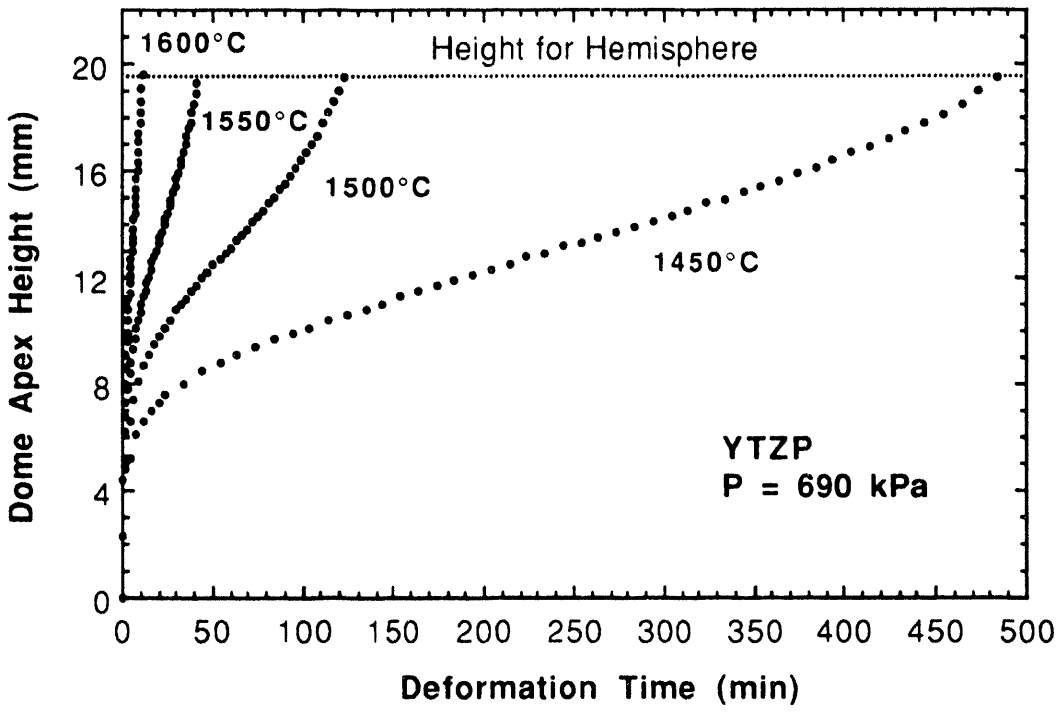

Fig.3.2 Deformation-time curves for superplastic gas-pressure forming of YTZP.

For the testing conditions employed in this investigation, the relationship between flow stress and dome apex height has been calculated and is shown in Fig.3.3. For discussion purposes, a *nominal* flow stress was selected through numerical integration of the curves shown in Fig.3.3 – using a height of 5 mm as the lower limit of integration. Note in Fig.3.3 that for each forming pressure used, the predicted shell stress is closely approximated by a single nominal flow stress for a large portion of the test. This corresponds to the "steady-state" deformation (region 2) observed in the deformation-time plots presented in Fig.3.2. The calculated results presented in Fig.3.3 show that the imposed flow stress levels for the experiments of this study spanned the range of 3.75 MPa to 30 MPa. For each hemisphere formed, an average strain rate was calculated by simply dividing the final true apex thickness strain by the duration of the test. (It is clear that the strain rate changes continuously during the forming experiment for the constant forming pressure condition. The determination of average strain rate, therefore, provides only a first-order result.) In this manner, the forming stress–strain rate data are presented graphically as a log–log plot in Fig.3.4.

The data indicate that, at all temperatures, the average strain rate $\dot{\varepsilon}$, is proportional to the nominal flow stress raised to the nth power, i.e.:

$$\dot{\varepsilon} = B \cdot \sigma^n \qquad (1)$$

The data of Fig.3.4 exhibit a stress exponent n of 2 for the tests conducted at high applied pressure with n increasing to a value of 3 at lower applied stresses. A stress exponent of 1 in the low stress (or low strain rate) region is in agreement with results previously obtained from uniaxial tension tests (without compensating for dynamic grain growth during deformation). An increasing stress exponent in the low stress region has been observed previously in superplastic YTZP and was attributed to dynamic grain growth.

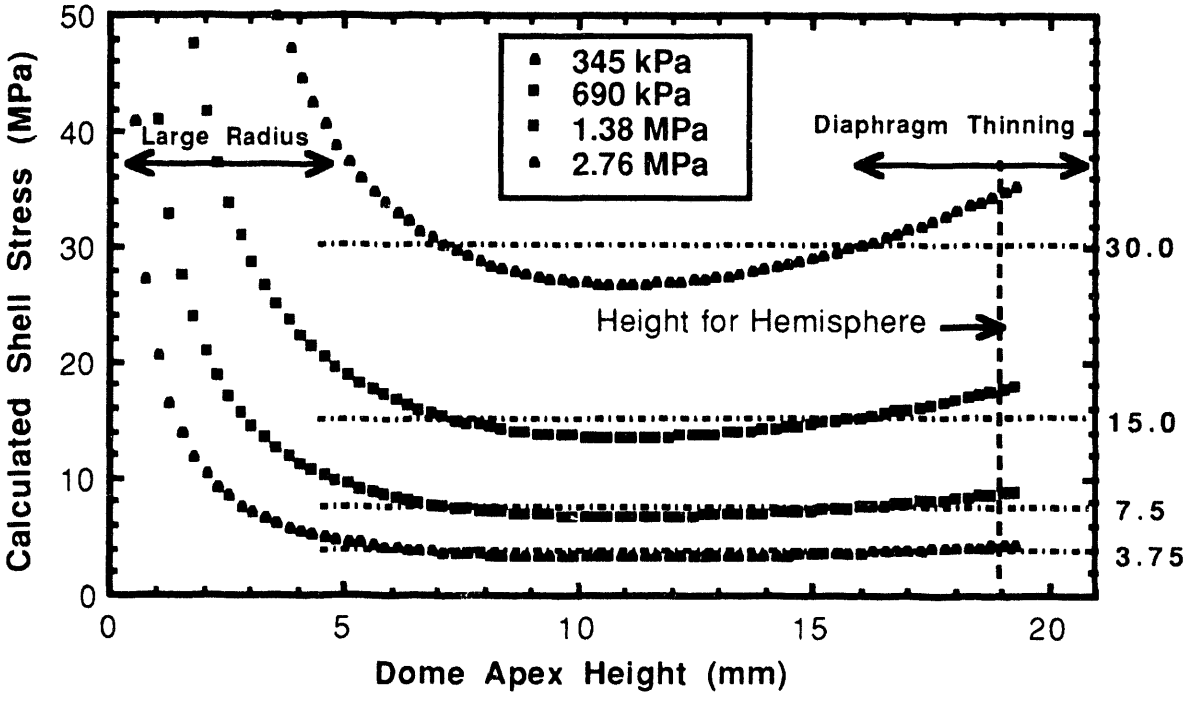

Fig.3.3 The relationship between shell stress and dome apex height.

A direct comparison between the strain rate–stress data obtained from the present biaxial forming experiments and those from uniaxial tests shown in Fig.3.5. It is particularly pointed out that the nominal shell stress for the biaxial tests used in Fig.3.4 is, in fact, a tangential stress. For the case of biaxial forming, both a tangential and an equal circumferential stress act at the dome apex (the thickness stress is zero). The effective stress, as used in Fig.3.4, acting on the dome apex is the resultant of these two stresses, which equals $\sqrt{2}$ times the stress value indicated in Fig.3.4. It is evident

in Fig.3.5 that, despite the fact that the strain rate from the biaxial forming test is generally faster than that from the uniaxial tests, both sets of data indicate a slightly decreasing stress exponent in the high strain rate region.

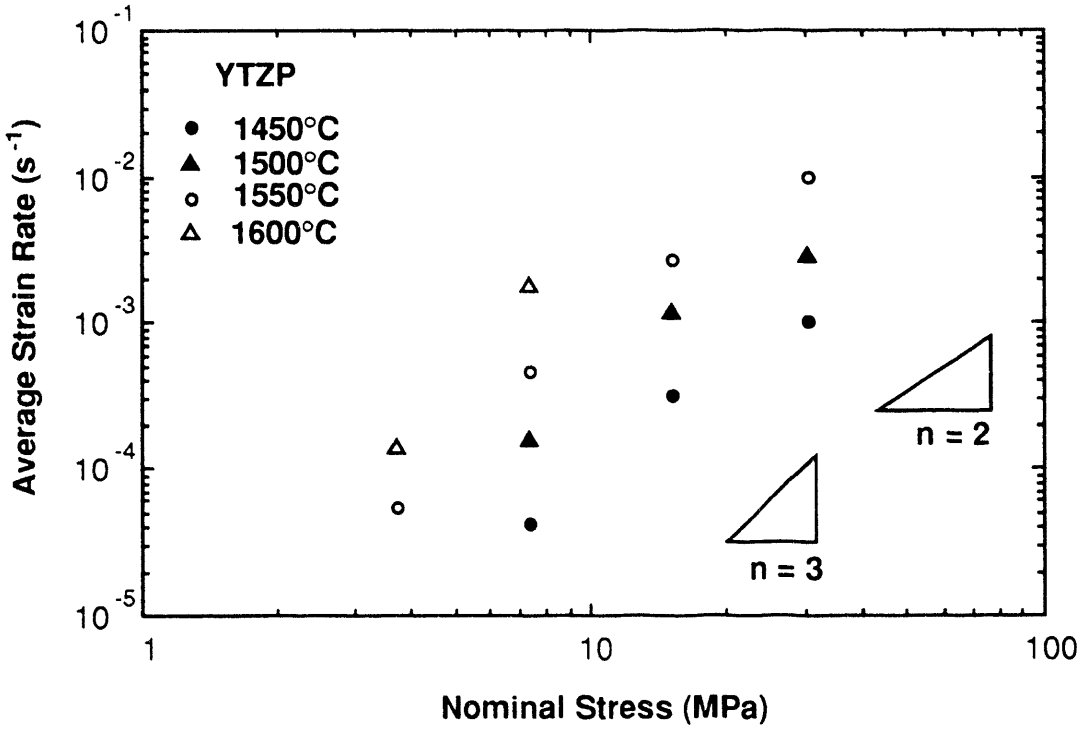

Fig.3.4 Average strain rate versus nominal stress.

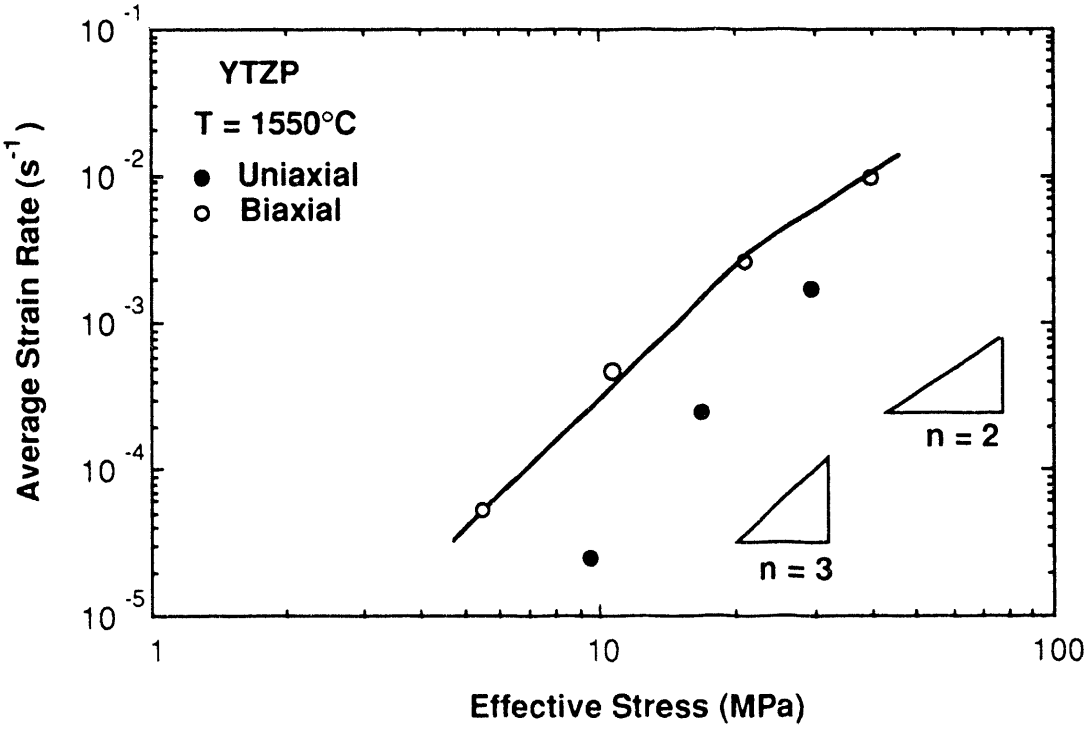

Fig.3.5 A direct comparison between data from biaxial and uniaxial tests.

III-4.2 Alumina/YTZP

In the case of Al_2O_3/YTZP, the hemispheres were deformed at temperatures between 1450 and 1600°C, and at forming pressures of 345 and 690 kPa. For these forming pressures and temperatures, 20%Al_2O_3/YTZP discs could be readily deformed into hemispherical caps over times ranging from 10^3 to 2 x 10^4 s.

The biaxial forming behavior for Al_2O_3/YTZP sheet is similar to that for YTZP. Namely, the forming curves essentially consist of three distinct regions. The experimental results indicate that the n value is approximately in the range from 2 to 3; n is 3 at 1500°C, but decreases to about 2 at 1550°C. These n values are in the usual range for superplastic ceramics. Again, data from the biaxial tests can be well correlated with that from the uniaxial tests. The strain rate from the biaxial forming test is about 3-4 times faster than that from the uniaxial tests; this result is similar to that found in YTZP.

III-4.3 Silicon

Silicon is difficult to deform because of its diamond structure (covalent). Although some reported hot hardness data indicated that Si softens at about 600-800°C, the tensile ductility of Si becomes appreciable only at temperatures above 1300°C (melting point of Si is 1414°C!) [14]. Net-shape forming of Si using casting techniques poses a major technical challenge because of strong chemical reactions between molten silicon and most crucible materials. In addition, Si virtually reduces the melting points of any chemical constituent. However, by proper selection of the mold material, the release agent for the mold, and the applied gas pressure, we have successfully formed single-crystal Si wafers into dome shapes [15]. A Si dome formed at 1375°C is shown in Fig.3.6. This dome is noted to exhibit a textured appearance, resulting from the constrained deformation of the single crystal.

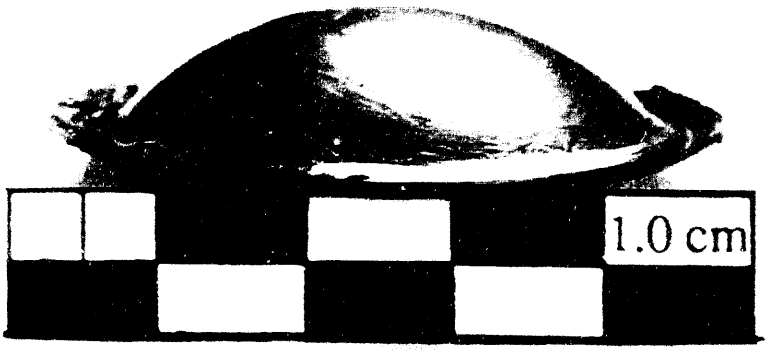

Fig.3.6 A silicon dome biaxial formed at 1375°C.

III-4.4 Hybrid YTZP/C103 (SPF/DB)

A combination of superplastic deformation with diffusion bonding offers the opportunity to manufacture a range of useful engineering structures. As an example of the potential for manufacturing metal-ceramic hybrids, the diffusion bonding and co-deformation of a YTZP ceramic disc and the Nb-based refractory alloy C-103 (nominal composition: Nb-10Hf-1Ti.) has been evaluated [16]. Alloy C-103 is a single-phase solid solution strengthened Nb alloy commonly used in spacecraft propulsion systems. Discs of YTZP and C-103 were assembled into the biaxial gas-pressure deformation apparatus and co-deformed at 1500°C. The hybrid assembly was successfully made. Such a thin-walled engineered metal-ceramic structure could have great utility in high thermal flux applications.

III-5 SUMMARY

In the past decade, ceramic superplasticity has rapidly advanced from a period of fundamental laboratory study to a level at which ceramic articles may be formed superplastically by gas pressure deformation. Using the technology developed for the present study, it is now possible to make intricately shaped, net shaped parts from superplastic ceramic sheet. Examples of a cone-on-cylinder geometry, a hat section, and a hemisphere are shown in Fig.3.7. Various shape geometries are possible with this process – as determined by the shape of the die. Continued studies are needed to understand the relationships between deformation variables (pressure, temperature) and deformation behavior (forming rate, strain distribution, cavitation).

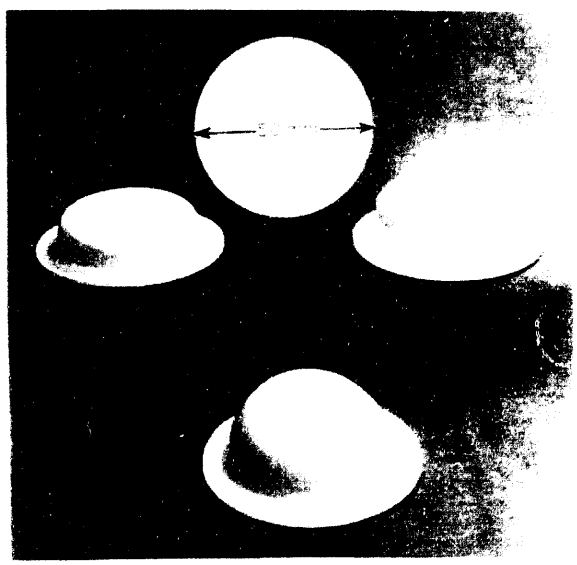

Fig.3.7 Examples of a cone-on-cylinder geometry, a hat section, and a hemisphere.

III-6 ACKNOWLEDGMENT

The financial support of this work was provided by the Army Research Office. The technical direction of Dr. Wilbur Simmons whose interest and enthusiasm for this project have been of great encouragement. The authors would also like to thank Dr. J.P. Wittenauer for his technical contributions.

III-7 REFERENCE

1. R.W. Rice, in *High Temperature Oxides, Refractory Materials 5-111*, ed. by A.M. Alper, New York, Academic Press, 1970, pp. 235-280.

2. T.G. Nieh and J. Wadsworth, *Scripta Metall. Mater.*, **24**, 763 (1990).

3. T.G. Nieh, D.L. Yaney, and J. Wadsworth, *Scripta Metall.*, **23**, 2007 (1989).

4. D.J. Schissler, A.H. Chokshi, T.G. Nieh, and J. Wadsworth, *Acta Metall. Mater.*, **39**, 3227 (1991).

5. A.H. Chokshi, T.G. Nieh, and J. Wadsworth, *J. Am. Ceram., Soc.*, **74**, 869 (1991).

6. F. Wakai, S. Sakaguchi, and Y. Matsuno, *Adv. Ceram. Mater.*, **1**, 259 (1986).

7. F. Wakai, S. Sakaguchi, and H. Kato, *J. Ceram. Soc. Jap.*, **94**, 72 (1986).

8. B. Kellett, P. Carry, and A. Mocellin, *J. Amer. Ceram. Soc.*, **74**, 1922 (1990)

9. F. Wakai, *Brit. Ceram. Trans.* , **88,** 205 (1989).

10. X. Wu and I.W. Chen, *J. Am. Ceram. Soc.*, **73,** 746 (1990).

11. J.P. Wittenauer, T.G. Nieh, and J. Wadsworth, *Scripta Metall. Maters.*, **26,** 551 (1992).

12. J.P. Wittenauer, T.G. Nieh, and J. Wadsworth, *J. Amer. Ceram. Soc.*, **76**, 1665 (1993).

13. O.D. Sherby, unpublished work (1993).

14. D.W.Lillie, *Trans.TMS-AIME*, p.249, April 1958.

15. *Lockheed Independent Research Report, no. LMSC-P049000*, pp. 4-185 to 4-193 (1992).

16. J.P. Wittenauer, T.G. Nieh, and J. Wadsworth, in *Processing and Fabrication of Advanced Materials*, ed. J.J. Morris, The Minerals, Metals & Materials Society, Warrendale, PA, (1994). (in press)

END

DATE
FILMED
3/7/94